AD-A114 816 PENNSYLVANIA STATE UNIV UNIVERSITY PARK APPLIED RESE--ETC F/6 9/1
THE PREDICTION OF TRANSDUCER ELEMENT PERFORMANCE FROM IN-AIR ME--ETC(U)
JAN 82 M E SCHAFER N00024-79-C-6043
UNCLASSIFIED ARL/PSU/TM-82-62 NL

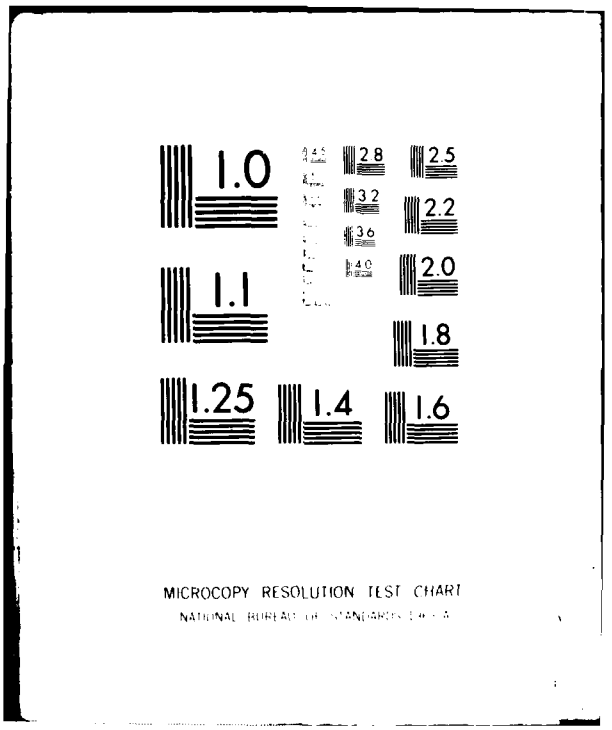
1.0
1.1
1.25
1.4
1.6
1.8
2.0
2.2
2.5
2.8
3.2
3.6
4.0
MICROCOPY RESOLUTION TEST CHART

(6)

THE PREDICTION OF TRANSDUCER ELEMENT PERFORMANCE FROM IN-AIR MEASUREMENTS

Mark Evan Schafer

Technical Memorandum
File No. TM 82-62
January 19, 1982
Contract No. N00024-79-C-6043

Copy No. 9

The Pennsylvania State University
Intercollege Research Programs and Facilities
APPLIED RESEARCH LABORATORY
Post Office Box 30
State College, PA 16801

NAVY DEPARTMENT
NAVAL SEA SYSTEMS COMMAND

UNCLASSIFIED

SECURITY CLASSIFICATION OF THIS PAGE *(When Data Entered)*

REPORT DOCUMENTATION PAGE		READ INSTRUCTIONS BEFORE COMPLETING FORM
1. REPORT NUMBER TM 82-62	2. GOVT ACCESSION NO. AD-A117 816	3. RECIPIENT'S CATALOG NUMBER
4. TITLE *(and Subtitle)* THE PREDICTION OF TRANSDUCER ELEMENT PERFORMANCE FROM IN-AIR MEASUREMENTS		5. TYPE OF REPORT & PERIOD COVERED M.S. Thesis, May 1982 6. PERFORMING ORG. REPORT NUMBER TM 82-62
7. AUTHOR(s) Mark Evan Schafer		8. CONTRACT OR GRANT NUMBER(s) N00024-79-C-6043
9. PERFORMING ORGANIZATION NAME AND ADDRESS The Pennsylvania State University Applied Research Laboratory, P.O. Box 30 State College, PA 16801		10. PROGRAM ELEMENT, PROJECT, TASK AREA & WORK UNIT NUMBERS
11. CONTROLLING OFFICE NAME AND ADDRESS Naval Sea Systems Command Department of the Navy Washington, DC 20362		12. REPORT DATE January 19, 1982 13. NUMBER OF PAGES 105 pages & figures
14. MONITORING AGENCY NAME & ADDRESS*(if different from Controlling Office)*		15. SECURITY CLASS. *(of this report)* Unclassified, Unlimited 15a. DECLASSIFICATION/DOWNGRADING SCHEDULE

16. DISTRIBUTION STATEMENT *(of this Report)*

Approved for public release, distribution unlimited,
per NSEC (Naval Sea Systems Command), 6/23/81.

17. DISTRIBUTION STATEMENT *(of the abstract entered in Block 20, if different from Report)*

18. SUPPLEMENTARY NOTES

19. KEY WORDS *(Continue on reverse side if necessary and identify by block number)*

thesis, transducer, element, performance, prediction

20. ABSTRACT *(Continue on reverse side if necessary and identify by block number)*

A technique has been developed which accurately predicts the performance of underwater acoustic arrays prior to array construction. The technique is based upon the measurement of lumped-parameter equivalent circuit values for each element in the array, and is accurate in predicting the array transmit, receive and beam pattern response.

The measurement procedure determines the shunt electrical and motional circuit elements from electrical immittance measurements. The electromechanical

DD FORM 1 JAN 73 1473 EDITION OF 1 NOV 65 IS OBSOLETE

UNCLASSIFIED

SECURITY CLASSIFICATION OF THIS PAGE *(When Data Entered)*

20 transformation ratio is derived from in-air measurements of the radiating face velocity and the input current to the transducer at resonance. The equivalent circuit values of a group of Tonpilz-type transducers were measured, and the self and mutual interaction acoustic loadings for a specific array geometry were calculated. The response of the elements was then predicted for water-loaded array conditions.

Based on the predictions, a selection scheme was developed which minimized the effects of inter-element variability on array performance. The measured transmitting, receiving and beam pattern characteristics of a test array, built using the selected elements, were compared to predictions made before the array was built. The results indicated that the technique is accurate over a wide frequency range.

ABSTRACT

A technique has been developed which accurately predicts the performance of underwater acoustic arrays prior to array construction. The technique is based upon the measurement of lumped-parameter equivalent circuit values for each element in the array, and is accurate in predicting the array transmit, receive and beam pattern response.

The measurement procedure determines the shunt electrical and motional circuit elements from electrical immittance measurements. The electromechanical transformation ratio is derived from in-air measurements of the radiating face velocity and the input current to the transducer at resonance. The equivalent circuit values of a group of Tonpilz-type transducers were measured, and the self and mutual interaction acoustic loadings for a specific array geometry were calculated. The response of the elements was then predicted for water-loaded array conditions.

Based on the predictions, a selection scheme was developed which minimized the effects of inter-element variability on array performance. The measured transmitting, receiving and beam pattern characteristics of a test array, built using the selected elements, were compared to predictions made before the array was built. The results indicated that the technique is accurate over a wide frequency range.

TABLE OF CONTENTS

TABLE OF CONTENTS (Continued)

LIST OF FIGURES

LIST OF FIGURES (Continued)

LIST OF TABLES

LIST OF SYMBOLS

B = susceptance, imaginary part of the admittance

c = sound speed, meter/second

C = capacitance, farads

C_m = mechanical compliance, meter/newton

D_z = diamter of admittance loop

E = electric potential, volts

F = mechanical potential or force, newtons

G = conductance, real part of the admittance

I = electric current, amps

j = square root of minus one

k = wave number, ω/c, meter^{-1}

k_{eff} = effective electromechnical coupling coefficient

L = inductance, henries

M_e = free-field voltage sensitivity, volts/μPa

M_i = free-field current sensitivity, amp/μPa

M_m = mechanical mass, kilograms

P = acoustic pressure, newtons/meter^2

Q_m = mechanical quality factor

R = resistance, real part of the impedance

R_e = ratio of model output voltage to input pressure

R_i = ratio of model output current to input pressure

S = area of the transducer face, meter^2

S_e = transmitting voltage response, μPa/volt

S_i = transmitting current response, μPa/amp

LIST OF SYMBOLS (Continued)

T_e = ratio of model output volume velocity to input voltage

T_i = ratio of model output volume velocity to input current

U = mechanical velocity, meter/second

V = volume velocity, $meter^3$/second

X = reactance, imaginary part of the impedance

Y = admittance

Z = impedance

η = transducer efficiency

λ = wavelength, meters

ρ = density, $kilograms/meter^3$

ϕ = electromechanical coupling coefficient, newtons/volt

ω_y = resonance frequency

ω_z = antiresonance frequency

$\omega_{1,2}$ = half power frequencies

ACKNOWLEDGMENTS

The author would like to express his sincere gratitude to his thesis committee composed of Dr. W. Jack Hughes, Dr. Paul M. Kendig, and Dr. William Thompson, Jr. for their valuable time and advice. Special thanks goes to Dr. Hughes, thesis advisor, for his assistance and guidance throughout this project, and to Mrs. Donna Schafer, for her patience and encouragement.

He would also like to acknowledge the financial support and assistance given him by the Applied Research Laboratory of the Pennsylvania State University under its contract with the Naval Sea Systems Command.

CHAPTER 1

INTRODUCTION

1.1 Problem Definition

Underwater acoustic arrays are frequently comprised of a number of individual piezoceramic transducer elements, each of which is electrically independent. The array output is the shaded (weighted) sum of the output of each of the elements. Since the transmitting and receiving characteristics of an array are dependent upon the characteristics of the individual array elements, much of the design of underwater acoustic arrays focusses on the design and testing of the transducer elements.

Due to a lack of an adequate prediction tool, the design of elements for an array is often an educated "cut-and-try" approach, involving the construction of test arrays. The problem stems from difficulties encountered in predicting the response of the elements prior to array assembly. Current in-air measurement procedures do not provide enough information to generate model parameters capable of the inclusion of a changeable acoustic loading. Air and water loading are very different, and the element response varies considerably with the change in medium. Further, the loading is affected by mutual interactions

between elements, making element loading a function of position within the array. Thus an element operating singly will perform differently when operating within an array. Because of this, it has not been possible to accurately predict an element's performance within an array, prior to assembly, without construction of test arrays.

Beam pattern response is another area of concern in the array design process. The array shading coefficients have the effect of shaping the beam pattern of the array. Varying the shading coefficients changes the beam pattern. The coefficients are altered by the variation in response of each element. In order to minimize the effects of element selection and placement upon the array shading, all of the elements should have similar response characteristics. However, due to variations in assembly such as glue joint thicknesses and alignment problems, no two elements will have exactly the same response. These response variations manifest themselves in the array as a degradation of the beam pattern. The use of elements with poor response uniformity results in increased sidelobe levels in the beam pattern.

Kendig[1] proposed a method for reducing the sidelobe levels in arrays. He devised a "scheme" for placing the elements within the array in order to cancel out the

variations in element performance. The "scheme" is theoretically sound, but the method suffers from some practical drawbacks, especially in the prediction of element performance. Although Kendig developed a means of comparing elements to one another, the comparison is valid only at the transducer's resonances, and is further handicapped by a number of simplifications and assumptions. Even so, this method has been used to produce arrays with lower sidelobe levels than arrays built with a random selection process.

A method capable of predicting the response of transducer elements within an array is needed in order to overcome the drawbacks in the current design and selection process; such a method is described in this study.

1.2 Goals of the Study

Using interactive computer techniques, this study provides an automated means for measuring transducer elements, predicting their responses when used within an array, and using this information in the Kendig selection scheme and in the prediction of array response. The specific objectives of this thesis are :

1. Analyze the piezoelectric transducer element in terms of a lumped parameter equivalent circuit model, capable of including radiation loading effects.
2. Develop a means for automatic analysis of elements in terms of the equivalent circuit parameters.

3. Generate response characteristics for each transducer, having included acoustic radiation and mutual interaction effects.

4. Use the response characteristics to find the total response for an array of elements.

5. Use the response characteristics to improve the Kendig selection process for assigning array locations to a given set of elements.

6. Use the response characteristics to predict the array beam pattern response for an array of elements.

The first topic is discussed in Chapter Two; readers already familiar with the lumped-parameter equivalent circuit model may choose to skip over this section. Chapter Three discusses the second point, and the remaining topics are covered in Chapter Four.

CHAPTER 2

THE EQUIVALENT CIRCUIT MODEL

2.1 Background

A common type of transducer used in underwater acoustics is the "Tonpilz" - from the German words for sound and mushroom. Figure 1 shows the structure of the transducer. Many equivalent circuit model analyses have been done using distributed parameters,[2,3] and are useful in the design of the transducer element. The circuit is valid over a wide frequency range, and clearly shows design tradeoffs. However, the circuit element parameters cannot be inferred from tests of the assembled element, and cannot account for assembly problems such as misalignment and improper glue joints. Thus, the distributed parameter model would not be suitable for the purposes of this study.

The lumped-parameter equivalent circuit model is valid over a much smaller frequency range around the transducer's mechanical resonance; since it "lumps" the effects of the individual transducer components together, it is somewhat less useful in the design phase. However, the equivalent circuit element parameters can be derived from tests of the assembled transducer. Further, the transducers are commonly used near or below their fundamental resonance

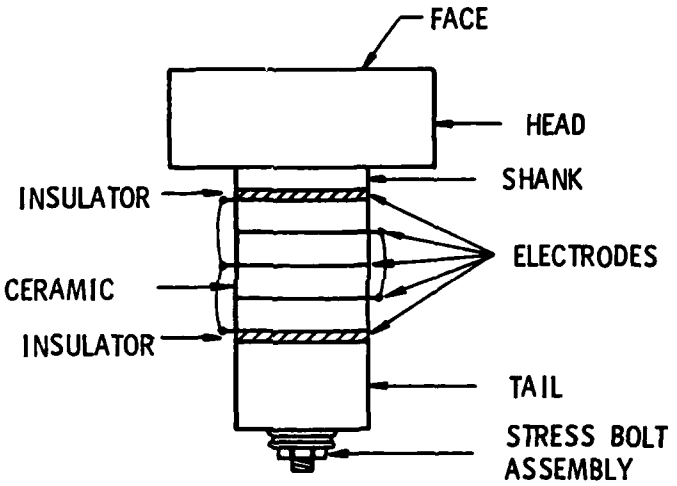

Figure 1. "Tonpilz"-Type Transducer

frequency, where the equivalent circuit is valid. For those reasons, the lumped parameter equivalent circuit model will be used.

A common starting point in the equivalent circuit analysis[4] is a simple block of piezoelectric material, one quarter wavelength thick, one face rigidly mounted and the other radiating into the medium. The analysis leads to an equivalent circuit, but the values of the parameters derived are not suitable to the Tonpilz configuration. Cherpak[5] has done an analysis of different Tonpilz type transducers, but again, the results neither predict nor account for the element variability found in actual practice.

Our purpose, then, is to derive the lumped-parameter equivalent circuit, and to put the values of the parameters in terms of measurements conducted on assembled units. From the references cited, we can be confident that the circuit is topologically correct; tests will later show the validity of the model in simulating actual element performance.

2.2 Assumptions and Limitations

In order to derive a model of the transducer, it is necessary to make some assumptions about the transducer's behavior and structure. Attempting to model the transducer completely would lead to an unnecessarily complex and

unwieldy equivalent circuit. Further, the model circuit elements are to be derived from measurements of actual transducers. The number of suitable measurements poses a limit on the number of circuit elements in a model that can be adequately derived. Therefore, certain assumptions and restrictions will be made on the model. Imposing restrictions generates limitations on the model's accuracy and suitability to the array design process.

The following restrictions apply to the model of the element's performance:

1. The entire circuit will be linear, passive, and reciprocal.
2. The mechanical domain can be treated as a simple mechanical oscillator (one degree-of-freedom).
3. The radiating face of the transducer has a fixed velocity distribution (one degree-of-freedom).
4. The electrical domain has little dissipation.

The first restriction limits the possible model elements to pure resistances, capacitances, and inductances in the electrical domain, and to pure springs, masses, etc., in the mechanical and acoustical domains. Although it will become apparent that linear elements are not able to completely model the transducer's behavior over a wide frequency range, they are sufficient over the range of interest, up to the fundamental resonance. By limiting the analysis to linear elements, the transducer's behavior can

be described by sets of linear differential equations. For the harmonic steady state, the linear differential equations may be transformed into linear algebraic equations in the frequency domain. Because of this, the circuit variables will be complex phasors, and the the circuit element values will be complex impedances.

The second restriction limits the model to a single mechanical resonance.* However, since transducers are typically operated only below or near that resonance, providing for more degrees-of-freedom and resonances does not significantly increase the model's accuracy. The additional degrees-of-freedom would account for such things as higher harmonics of the fundamental, transverse vibrations, and spurious resonances. These generally are not of great concern nor are they easily measured.

The third assumption requires that the transducer's radiating face moves as a rigid piston. Therefore this model will not treat a transducer with head flap.[6]

The final restriction is true for transducers of interest, constructed of piezoceramic material. One problem with including electrical losses is that they are hysteretic, and therefore nonlinear. If linearized over some frequency range, the loss turns out to be small enough

*It will be shown how additional degrees-of-freedom and resonances can be added.

to neglect in comparison to other circuit elements. The implications of this restriction will be discussed further in the sections dealing with measurement procedures.

A generalized linear equivalent circuit model of the transducer can be generated from a simple consideration of the transducer's function. The function of a transducer is the conversion of energy from the acoustical domain to the electrical, and vice versa. In the case of piezoelectric transducers, acoustical energy is first converted to mechanical energy; mechanical energy is then converted into electrical energy. It is necessary for the lumped-parameter equivalent circuit model of a piezoelectric transducer to account for the transducer's properties in the electrical, mechanical, and acoustic domains , as well as the transformations between these domains. With this in mind, Figure 2 is a generalized model of a transducer element. There are five two-port networks to represent the electrical, mechanical, and acoustical domains, and the two transformations between the domains. Note the different potential and flux variables used between the networks. This model will be made more specific in the next section, using the above restrictions.

2.3 Derivation of Model Circuit Elements

Starting with the generalized linear equivalent circuit model in Figure 2, the exact structure of each of

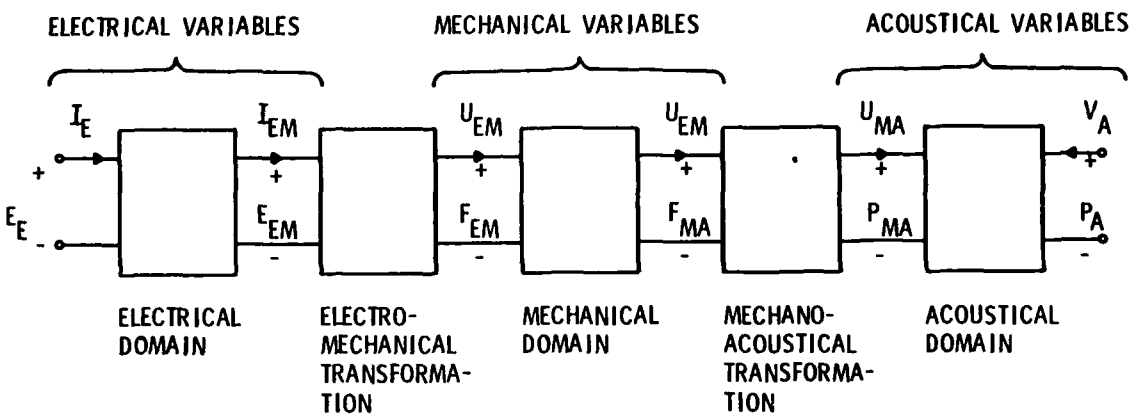

Figure 2. Generalized Equivalent Circuit Model

the networks can be determined from the above restrictions and an intuitive look at the transducer's construction.

The structure of the first network, representing the electrical domain, can be deduced from the physical structure of the transducer, Figure 1. Neglecting the piezoelectric properties of the ceramic, the electrodes form a simple parallel plate capacitor stack, with the ceramic serving as a dielectric material. The capacitance is a function of the number and area of the electrodes, and the thickness and dielectric constant of the ceramic sections. There is also a small dielectric loss from the conductance of the ceramic. The network representing the electrical domain consists of a capacitor in parallel with a resistor.

The capacitive property arises from the ability of a dielectric material to hold a potential charge across a pair of electrodes. The ceramic in a transducer, however, is both dielectric and piezoelectric. The charge across the ceramic therefore also causes a mechanical deformation in the material's crystalline structure, coupling the electrical and mehanical domains.

The equivalent circuit model for the electromechanical transformation is found by examining the nature of the piezoelectric phenomenon. Mechanically deforming a piezoelectric material causes a charge separation within

its crystalline structure. The voltage potential caused by the separation will vary with the orientation of the mechanical stress and voltage measurement with respect to the crystal polarization orientation. The voltage is a function of the size of the material, the amount of deformation, and the piezoelectric stress factor appropriate to the crystal polarization orientation. By including the compliance coefficient of the piezoceramic material into the expression, the transformation factor takes on the dimension of force/voltage, in units of Newtons/Volt. By further substitution, the ratio is equivalent to current/velocity (Amp/Meter/Second). The equivalent circuit element that expresses this type of transformation is an ideal transformer. Figure 3 shows the ideal transformer and the circuit relationships applicable to it. By convention, the electromechanical transformation factor is given the symbol ϕ, (A/M/Sec or N/V), and the turns ratio is expressed as $1/\phi:1$ or $1:\phi$, which is equivalent to letting C in Figure 3 equal $1/\phi$.

From the second restriction, the network representing the mechanical domain is a simple mechanical oscillator. The representation of a mechanical oscillator is the system shown in Figure 4A, consisting of a mass, a spring, and a dissipative element. Under the assumption that the dissipation is small, and is proportional to the velocity, the equivalent circuit for the mechanical system is shown

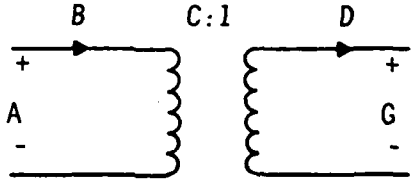

TRANSFORMATION RELATIONSHIPS

POTENTIAL: $G = A/C$

FLUX: $D = C/B$

IMPEDANCE: $G/D = \left(\frac{1}{C^2}\right)\left(\frac{A}{B}\right)$

STEP DOWN: $C > 1$

STEP UP: $C < 1$

Figure 3. The Ideal Transformer

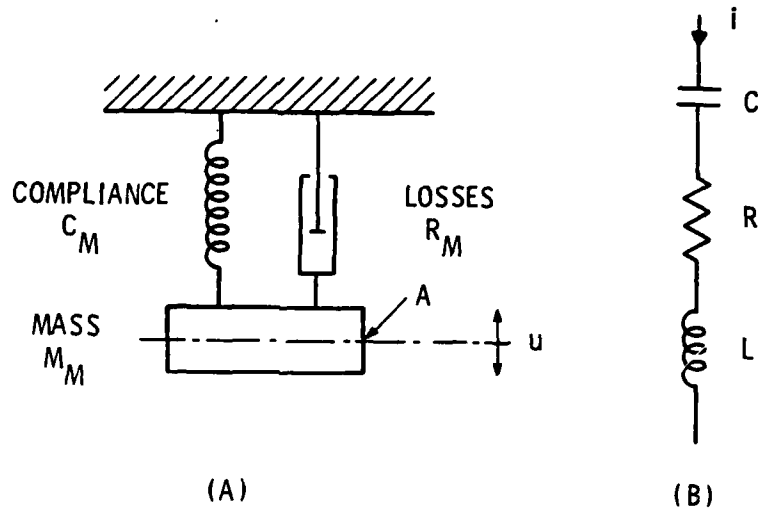

Figure 4A. A Mechanical Oscillator

Figure 4B. The Electrical Equivalent of a Mechanical Oscillator

in Figure 4B. The circuit elements are in series because the velocity of each element, measured at point A, is the same. Since velocity is the flux variable in the model, the same velocity must "flow through" each of the equivalent circuit elements. By connecting in parallel sections like the one shown, additional degrees-of-freedom and resonances may be added.

Anticipating the results of the next paragraph, the mechanoacoustical transformation is accomplished by the radiating face of the transducer. Under the assumption of "lumped" elements, and looking at Figure 1, the displacement generated by the ceramic elements must be equal to the displacement of the radiating face, taken with respect to the tail mass. U_{em} must equal U_{ma}. Therefore, the equivalent circuit for the mechanical domain in the model is shown in Figure 5.

The mechanoacoustic transformation is accomplished through the area of the radiating face of the element. A displacement of the face causes a change in volume in the acoustic medium: the velocity of the face U_{ma} produces a volume velocity V_a in the medium. Similarly, a force F_{ma} on the face becomes a force per unit area, or pressure P_a in the medium. Mathematically, this is expressed as

$$V_a = SU_{ma} \quad \text{and} \quad P_a = F_{ma}/S \tag{1}$$

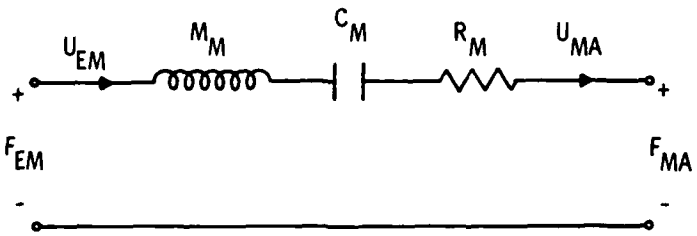

Figure 5. Mechanical Domain Equivalent Circuit

where S is the area of the face. The equivalent circuit representation for the mechanoacoustic transformation is an ideal transformer with a turns ratio of S:1, and S has the units of $Meters^2$.

The final network, representing the acoustical domain, cannot be strictly analysed as a combination of lumped circuit elements. The solution of the radiation loading on a flat piston is very complex, and is further complicated by mutual coupling effects in arrays. However, for a given frequency and array velocity distribution (shading pattern), there is a unique radiation loading on each element*, which may be represented as a generalized impedance Z_a. Figure 6 is the circuit representation for the acoustical domain. The power output of the transducer is proportional to the volume velocity through the real part of Z_a, labeled R_a.

Figure 7 then, is the lumped-parameter equivalent circuit model of a Tonpilz piezoelectric transducer.

2.4 Input/Output Equations for the Model

The lumped-parameter equivalent circuit model can be analysed by standard electrical network techniques to find the input/output equations of the transducer. Figure 8

*The techniques for finding the radiation loading and mutual coupling impedance are discussed in Appendices A and B, respectively.

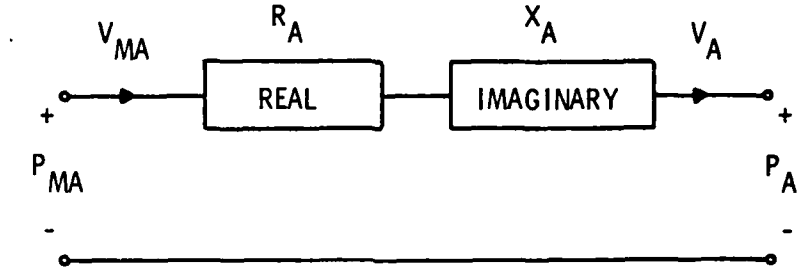

Figure 6. Acoustical Domain Equivalent Circuit

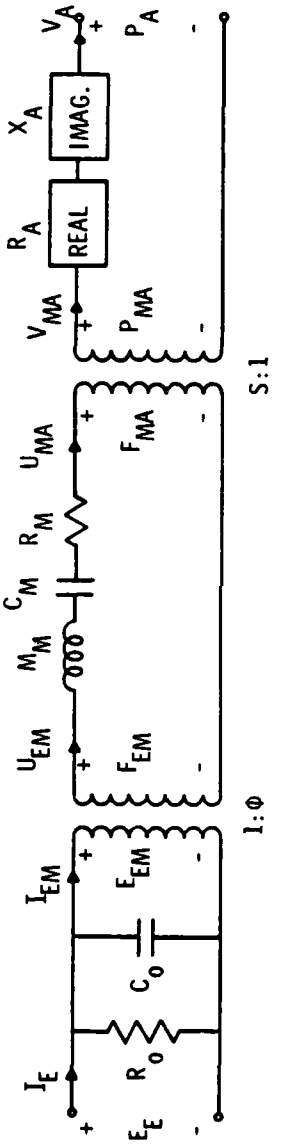

Figure 7. The Complete Equivalent Circuit

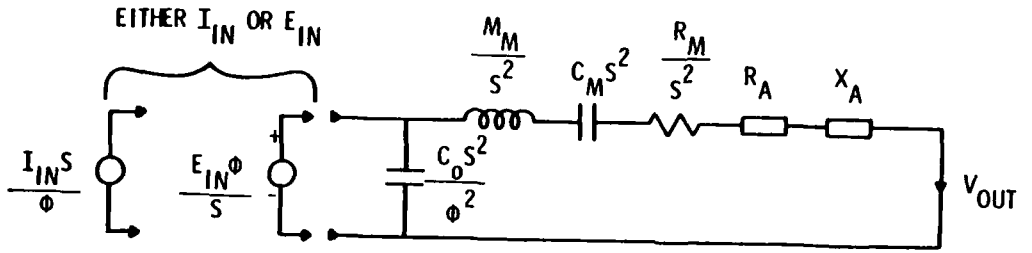

(A) TRANSFORMED TO ACOUSTICAL DOMAIN FOR TRANSMIT CASE

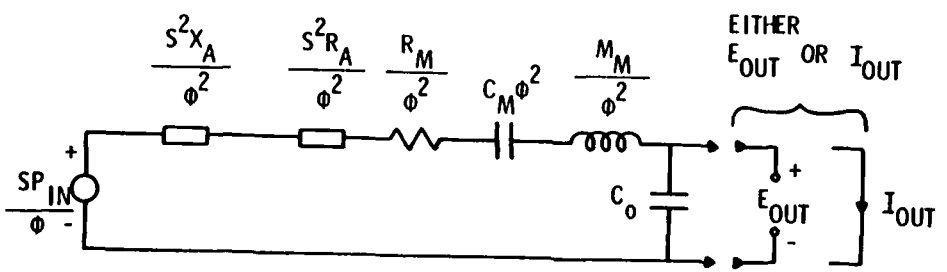

(B) TRANSFORMED TO ELECTRICAL DOMAIN FOR RECEIVE CASE

Figure 8. Equivalent Circuits for the Transmit and Receive Cases

results from removing the transformers by the appropriate multiplication. Figure 8A is the circuit for the transmit case and Figure 8B is for the receive case.

For the receive case, the measured electrical quantity can either be the open circuit voltage E_{out}, or the short circuit current I_{out}. Similarly, in the transmit case, the driving electrical source can be modelled either as an ideal voltage source E_{in}, or an ideal current source I_{in}. Although the acoustical domain cannot be considered either shorted or opened, the transmit and receive cases use different circuit parameters. In the receive case, the input variable is the pressure P_{in} at the face of the transducer; in the transmit case, the output variable is the volume velocity V_{out} produced by the transducer.

By convention, for the receive case, the output voltage and current sensitivities for the k^{th} transducer element may be expressed as

$$|R_e|_k = |E_{out}|/|P_{in}| \qquad |R_i|_k = |I_{out}|/|P_{in}| \tag{2}$$

Similarly, the transmit response may be written

$$|T_e|_k = |V_{out}|/|E_{in}| \qquad |T_i|_k = |V_{out}|/|I_{in}| \tag{3}$$

Since the derived equivalent circuit is reciprocal and passive, it can be shown that[7]

$$|R_i|_k = |T_e|_k \qquad |R_e|_k = |T_i|_k \tag{4}$$

Note that this is not the same as acoustic reciprocity, which includes a factor accounting for sound transmission into the medium.

Solving the equivalent circuit for the first pair yields

$$|R_i|_k = \frac{\omega C_m \phi S}{[(1-\omega^2 C_m M_m - \omega C_m S^2 X_a)^2 + \omega^2 C_m^2 (R_m + S^2 R_a)^2]^{\frac{1}{2}}} \tag{5}$$

$$\mathrm{Arg}(R_i)_k = \tan^{-1}\left\{\frac{\omega C_m (R_m + S^2 R_a)}{1 - \omega^2 C_m M_m - \omega C_m S^2 X_a}\right\}$$

If the transducer is operated at a frequency such that $\omega^2 C_m M_m - 1$ equals zero, then the equations reduce to

$$|R_i|_k = \phi S/[R_m^2 + 2R_m R_a S^2 + S^4 |Z_a|^2]^{\frac{1}{2}} \tag{6}$$

$$\mathrm{Arg}(R_i)_k = \tan^{-1}\{-[R_m + S^2 R_a]/S^2 X_a\}$$

where $|Z_a| = [R_a^2 + X_a^2]^{\frac{1}{2}}$. Solving the circuit for $(R_e)_k$ and $(T_i)_k$ yields

$$|R_e|_k = \frac{\phi S}{[(\phi^2 - \omega^2 C_o M_m + C_o/C_m - \omega C_o S^2 X_a)^2 + \omega C_o^2 (R_m + S^2 R_a)^2]^{\frac{1}{2}}} \tag{7}$$

$$\mathrm{Arg}(R_e)_k = \tan^{-1}\left\{\frac{\omega C_o (R_m + S^2 R_a)}{\phi^2 - \omega^2 C_o M_m + C_o/C_m - \omega C_o S^2 X_a}\right\}$$

If the transducer is operated at the frequency such that $1 - \omega^2 M_m C_o/\phi^2 + C_o/C_m \phi^2$ equals zero, then the equations simplify to

$$|R_e|_k = \phi S/(\omega C_o)[R_m^2 + 2R_m R_a S^2 + S^4 |Z_a|^2]^{\frac{1}{2}} \tag{8}$$

$$\mathrm{Arg}(R_e)_k = \tan^{-1}\{-[R_m + R_a S^2]/S^2 X_a\}$$

These are the input/output or transfer function equations for the transducer. Equations 5 and 7 will be used for predicting the amplitude and phase of the transducers in the array design process. The choice of the frequencies which reduced Equations 5 and 7 are not arbitrary: the frequencies will be shown to be the resonant and antiresonant frequencies, respectively.

2.5 The Reduced Model

For measurements of the electrical immittance properties of the transducer, the complete equivalent circuit model may be reduced to a more convenient form. If we assume that the transducer is measured in air, for which the radiation loads are relatively small, then R_a and X_a can be set to zero. Similarly, we can assume that there is no significant pressure field at the transducer face. Applying those assumptions to Figure 8B, we can rename the parameters as traditional electrical circuit elements. The results are shown in Figure 9, where

$$C_o = C_o \qquad C = C_m\phi^2 \qquad L = M_m/\phi^2 \qquad R = R_m/\phi^2 \tag{9}$$

This simple circuit is sufficient to describe the electrical immittance behavior of the transducer, with the assumption that R_a and X_a can be neglected.*

* This was tested as part of the experiments described in Section 3.2.

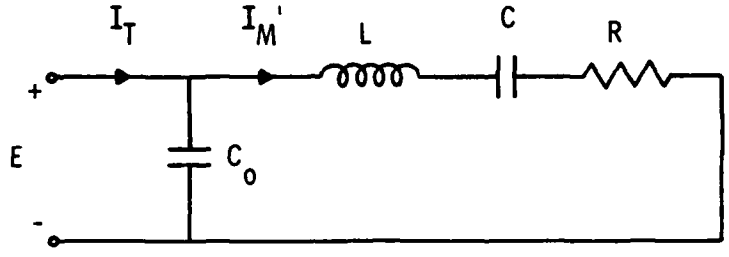

Figure 9. The Reduced Equivalent Circuit Model

It will be shown that all of the non-acoustic parameters in the complete equivalent circuit, except the transformation factor ϕ, can be found by treating the transducer as a one-port device. The technique for finding ϕ is discussed in Section 3.3.

2.6 One-Port Behavior of the Reduced Model

The reduced equivalent circuit model can be used to predict the electrical immittance response of the transducer over a frequency band around the resonance frequency. The values of the circuit elements can be found from measurements of the transducer's electrical properties, and relating the measurements to the predictions of the model. The following discussion will be limited to the reduced equivalent circuit model, as shown in Figure 9.

From the figure, the input electrical admittance of the transducer is:

$$Y = j\omega C_o + \frac{j\omega C(1 - LC\omega^2) + \omega^2 C^2 R}{(1 - LC\omega^2)^2 + \omega^2 C^2 R^2} \qquad (10)$$

This will show two resonances : one from the motional branch alone, and one from the coupled system. The motional resonance frequency is

$$\omega_y = 1/(LC)^{\frac{1}{2}} \qquad (11)$$

At this frequency, the admittance is

$$Y|_{\omega_y} = j\omega_y C_o + 1/R \tag{12}$$

The second, or antiresonance frequency is

$$\omega_z = [(C + C_o)/(LCC_o)]^{\frac{1}{2}} \tag{13}$$

The conductance of the transdcuer is a maximum at ω_y, the resistance of the transducer is approximately a maximum at ω_z. Note that Eqs. 11 and 13 are the same as the conditions used to reduce Eqs. 5 and 7.

Figure 10 shows the input admittance versus frequency for the model near the motional resonance. The susceptance curve is the sum of the admittance of the capacitor (the "blocked" susceptance) and the admittance of the motional branch. The conductance curve is due to the motional branch alone. The peak in the conductance curve occurs at the resonance frequency, ω_y. At this frequency, the motional susceptance goes to zero; from Eq. 12, the motional conductance G_y is just the inverse of the motional resistance element R.

The two frequencies labeled ω_1 and ω_2 are the half-power or quadrantal frequencies. Together with ω_y, the points define the Q_m, or quality factor of the motional branch, which is expressed as

$$Q_m = \omega_y/(\omega_1 - \omega_2) = f_y/(f_1 - f_2) \tag{14}$$

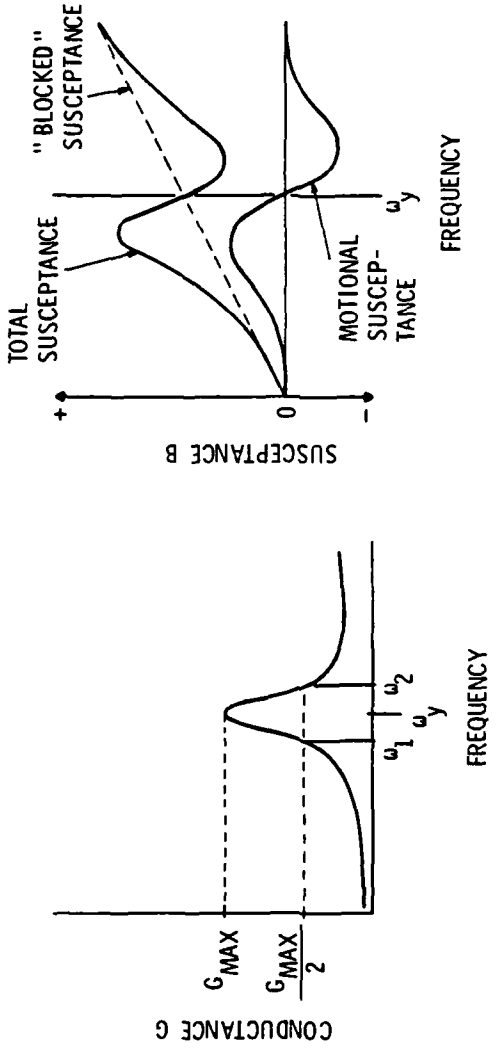

Figure 10. Typical Input Admittance Versus Frequency

From basic circuit theory, the Q_m may also be expressed in terms of the motional branch circuit elements:

$$Q_m = 1/\omega_y RC \tag{15}$$

In the absence of loading, the Q_m is a measure of the mechanical dissipation of the transducer at resonance. A higher Q_m implies a more efficient motional branch.

Another measure of a transducer's performance is the ratio of the energy stored in the motional branch to the total energy stored in the transducer. By examining the model at low frequencies, where the capacitive elements dominate the impedance, the electromechanical coupling coefficient, called k_{eff}, becomes obvious. From Figure 11, the energy in the motional branch is $(1/2)CV^2$, and the total energy stored is $(1/2)(C + C_o)V^2$. Therefore,

$$k_{eff} = [C/(C + C_o)]^{\frac{1}{2}} = [1 - (\omega_y/\omega_z)^2]^{\frac{1}{2}} \tag{16}$$

The above analysis has shown that the reduced equivalent circuit model has two resonances, at ω_y and ω_z. From those frequencies and the half-power points, the Q_m and k_{eff} are derived. Section 3.1 will discuss the experimental techniques for measuring transducers to find these parameters.

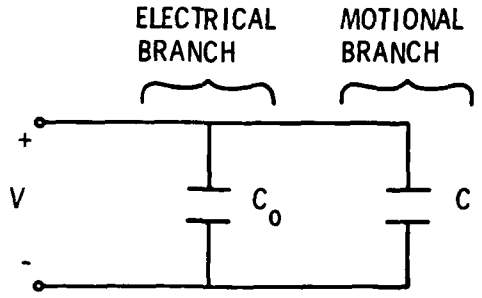

Figure 11. Low Frequency Reduced Model

CHAPTER 3

THE MEASUREMENT OF CIRCUIT PARAMETERS

3.1 Input Immittance Measurements

In the previous section, the input immittance behavior of the reduced equivalent circuit model was derived. Using Equation 10 as a starting point, the resonance and antiresonance frequencies, the Q_m, and the coupling coefficient were derived in Equations 11 through 16. The purpose of this section is the derivation of the equations needed to find the equivalent circuit values from measurements of input immittance.

From Equation 12, if B_y and G_y are the susceptance and conductance of the circuit at ω_y, then

$$R = 1/G_y \qquad \text{and} \qquad C_o = B_y/\omega_y \tag{17}$$

From the measurement of G_y and Q_m,

$$C = G_y/\omega_y Q_m \tag{18}$$

Finally, the value of the inductor, L, is derived from C and ω_y,

$$L = 1/\omega_y^2 C \tag{19}$$

These four equations are sufficient for analysis of the equivalent circuit model.

In practice, the circuit element values are found by a slightly different set of relations, for reasons of repeatability and ease of measurement. If the transducer element is measured at a low enough frequency, then the impedance is dominated by the capacitances. The low frequency susceptance is due to the combined effect of C and C_o. Therefore,

$$C + C_o = B/\omega \qquad \omega << \omega_y \tag{20}$$

This equation is used with Eq. 18 to find C_o, the shunt, or clamped capacitance.

Figure 12 is the equipment set-up used for the impedance measurement. The HP3750 Impedance Analyzer is designed to make insertion loss/gain and phase angle measurements on two-port devices. It was used to find the input immittance of one-port devices by use of a special input termination and use of the appropriate formulae stored in the calculator. The details of the termination and formulae are discussed in Appendix C. The HP9825B calculator was programmed to measure the admittance and impedance characteristics of the transducer element under test, and to calculate the equivalent circuit values for the element. The low frequency capacitance measurements

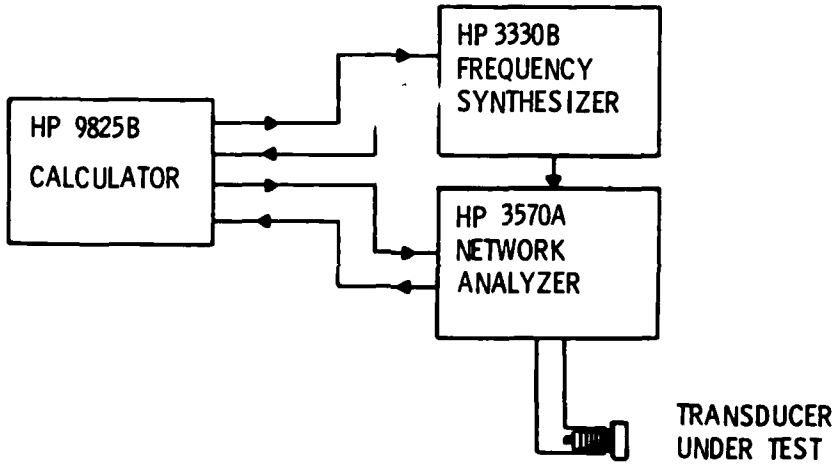

Figure 12. Experimental Set-up for the Impedance Tests

were taken at three frequencies near $\omega_y/20$, and then averaged. The frequencies ω_y and ω_z were found by sweeping over a specified frequency range, until the frequency of maximum conductance (ω_y) and the frequency of maximum resistance (ω_z) were located. The half-power frequencies were specified as the frequencies for which the conductance was one-half G_y. From these measurements, the calculator used Equations 17 through 20 to find the R, L, C, and C_o of the transducer element. The circuit element values were stored in the calculator memory for later use. Plots showing the magnitude and phase of the impedance versus frequency could also be made. The solid curve in Figure 13 is an example of a typical measured impedance plot.

To establish the reliability and repeatability of the measurements, many tests were repeated on a control group of transducer elements. Once mounting and measurement techniques were refined, a group of over 60 transducer elements were tested and the results stored for later use.

3.2 Verification of the Immittance Techniques

In order to verify the immittance measurements, a number of calibrations and built in self-checks are calculated.

The accuracy of the low frequency capacitance was verified using the impedance program to measure a number of

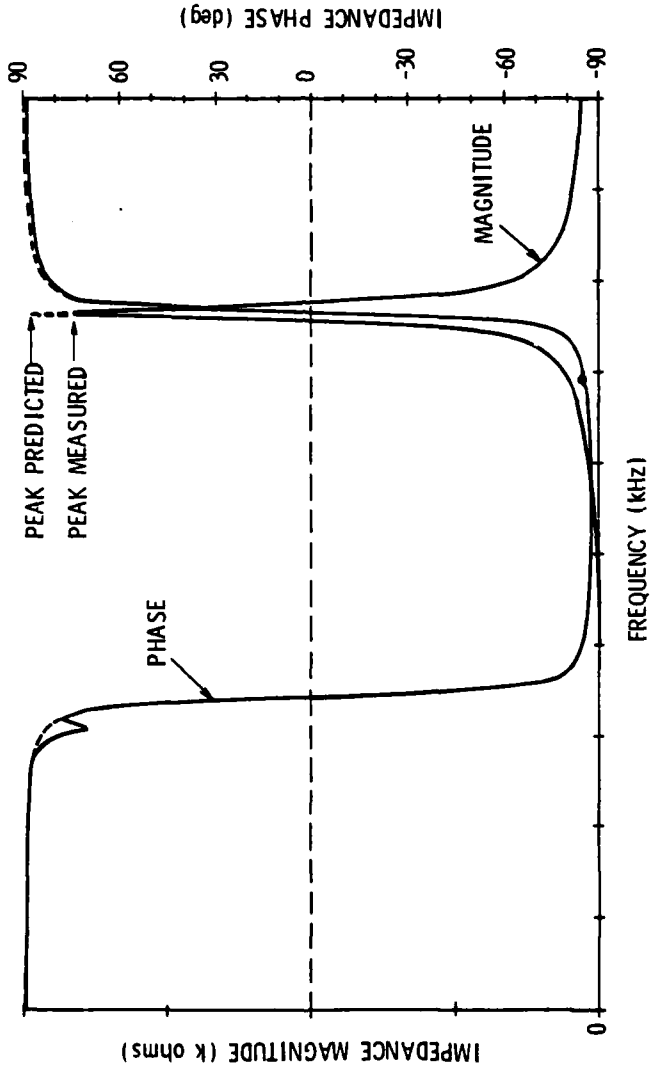

Figure 13. Predicted and Measured Transducer Impedance

capacitors, whose values were in the range of the transducer elements tested. The readings were found to be within $\pm$.6 percent of capacitance bridge measurements.

It was assumed in Section 2.5 that the acoustic radiation loading in air is sufficiently low that R_a and X_a could be set to zero. This was tested by placing elements in a bell jar, and measuring the immittance of the elements under atmospheric and low pressure conditions. The results indicated that air loading caused a .5 percent error in the measurement of R. There was no significant shift in the measured values of any of the other parameters of interest. It was therefore concluded that the assumption of negligible in-air loading was correct.

A self-check routine in the program calculated and printed the K_{eff} of the transducer using both terms of Eq. 16. By comparing the value from the capacitance measurements and the value from the ω_y and ω_z measurements, the self-consistency of the entire measurement was checked. The differences were typically less than .7 percent for most of the elements. This indicated the resonance frequency and the capacitance measurements were indeed consistent.

Some of the elements had a portion of the head mass removed to allow for better array geometry. These elements also had their tail masses changed or "trimmed" to

compensate for the shift in ω_y caused by the loss of head mass. These changes in mass caused the measured G_y and Q_m values to shift, and therefore changed the calculated value of C for the transducers. When the values of k_{eff} calculated from C and C_o were compared to values calculated from ω_y and ω_z, there was a discrepancy of 7 percent. An examination of the measured impedance plots revealed that these elements have an extra resonance slightly below ω_y, thus affecting their behavior near resonance. The equivalent circuit model as derived cannot account for the behavior of these elements, because of the extra resonance. Therefore caution was taken when interpreting the model's response prediction for these elements.

A second self-check routine had two complementary purposes: to test the accuracy of the measurement procedure, and to test the accuracy of the equivalent circuit model. To do this, the calculator was programmed using Equation 10 with the measured equivalent circuit values inserted. The immittance curves were redrawn using the lumped paramenter equivalent circuit. The results were both printed and plotted. The printed results showed that the technique could find the equivalent circuit element values to within .5 percent. The plots showed the the equivalent circuit accurately modeled the transducer's input impedance over a range near ω_y, as seen in Figure 13. The model was not as accurate in the range near ω_z, where

the predicted impedance was generally 30 percent higher than measured. This discrepancy arises from slight inaccuracies in the C_o measurement, and in the inaccuracies caused by neglecting R_o. Appendix D discusses the error caused by the removal of R_o, and suggests a technique for reducing it. It was found, however, that this error had little effect on the final results of the study.

3.3 Velocity-Current Measurements

The electromechanical transformation factor cannot be found by measurement of input electrical properties alone. Since the immittance measurement treats the transducer as a one-port device (Fig. 9), it cannot get at "both sides" of the electromechanical transformation. Therefore, it is necessary to measure some electrical and mechanical properties of the transducer simultaneously.

Referring to Figure 7, the electromechanical transformation factor can be expressed either as a voltage/force (E_{em}/F_m) or a current/velocity (I_{em}/U_m) ratio. Although the input voltage can be easily measured, the output force from the ideal transformer cannot; however, the velocity of the radiating face and the input current can be measured simultaneously. The current I_{em} in the standard circuit model is the same as the motional current I_m' in the the reduced circuit model. The reduced circuit model can be solved for the motional current I_m'

using the element values found by impedance measurements. The motional current, in terms of the electrical input current I_t, is:

$$|I_m'| = |I_t| / [(1 - \omega^2 C_o L + C_o/C)^2 + (\omega C_o R)^2]^{\frac{1}{2}}$$

$$\text{Arg}(I_m') = \text{Arg}(I_t) + \tan^{-1}[-\omega C_o R/(1 - \omega^2 C_o L + C_o/C)] \quad (21)$$

The current U_m out of the electromechanical transformer equals the current U_{ma} flowing into the mechanoacoustic transformer. This last transformer represents the transducer's radiating face ; on one side is the velocity of the mechanical domain, and on the other is the volume velocity of the acoustical domain. The two are related by the area of the face. In this case, only the velocity of the face, U_f, is of interest and not the volume velocity produced by the face. The current U_{ma} can be found by measuring the velocity of the face. If U_f is the measured face velocity, then the electromechanical transformation factor is

$$\phi = I_m' / U_f \quad (22)$$

The face velocity is determined from measurements of the face displacement amplitude. In the steady state, the two are related by the radian frequency. A non-contacting fiber optic probe is used to measure the displacement amplitude.[8] Figure 14 illustrates the principle of

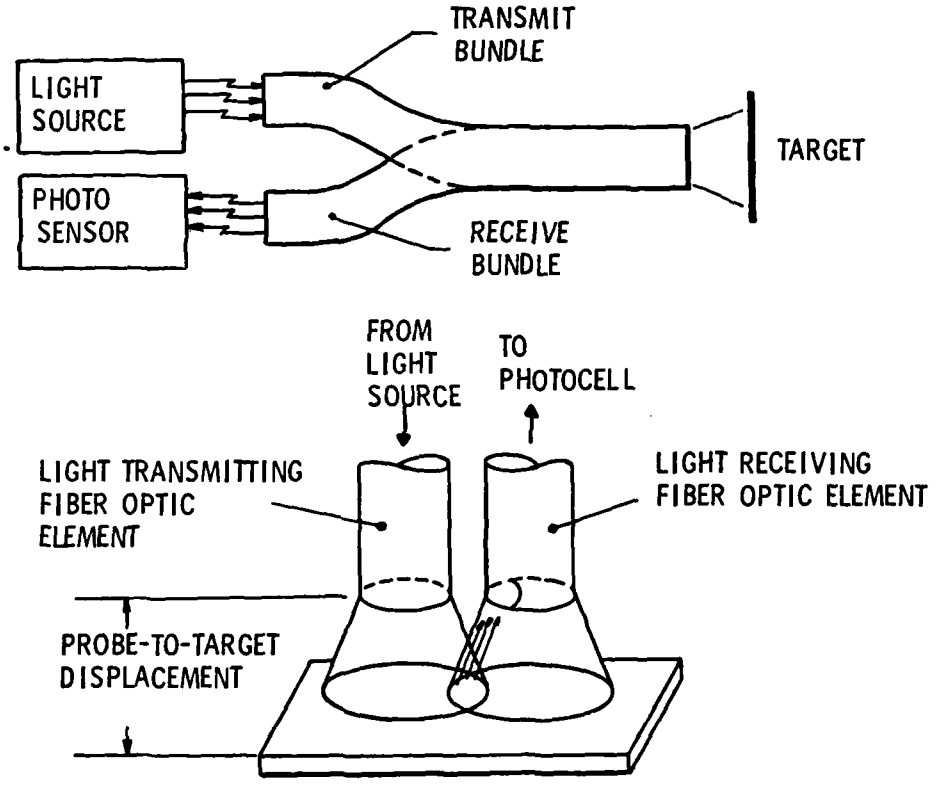

Figure 14. Principle of Operation of Fotonic Sensor

operation of the light fiber probe. As a test surface moves away from the probe tip, the area of overlap between the transmitted light cone and the received light cone increases. The sensor electronics convert the light amplitude signal from the probe into a voltage proportional to displacement. By differentiating the displacement signal, the velocity of the surface is measured.

Figure 15 shows the experimental set-up used to measure the transformation ratio. The transducers were mounted by their stress bolts; immittance measurements had shown that the method did not significantly alter the transducer's resonances. This mounting method also insured that the face displacement was the sum of the expansions of the ceramic sections, assuming that little of the displacement is taken up in compliant deformation of the head mass, the tail mass, and the stress bolt.

The input current to the transducer was measured by a current-to-voltage conversion coil. The unit has a sensitivity of .1 volt/ampere, and has sufficient frequency response to cover the range of interest.

The fiber optic probe was calibrated by using a calibrated positioner and a voltmeter. The probe tip was manually displaced in steps away from the transducer face, and simultaneously the voltage from the sensor unit was recorded at each step. This provided a

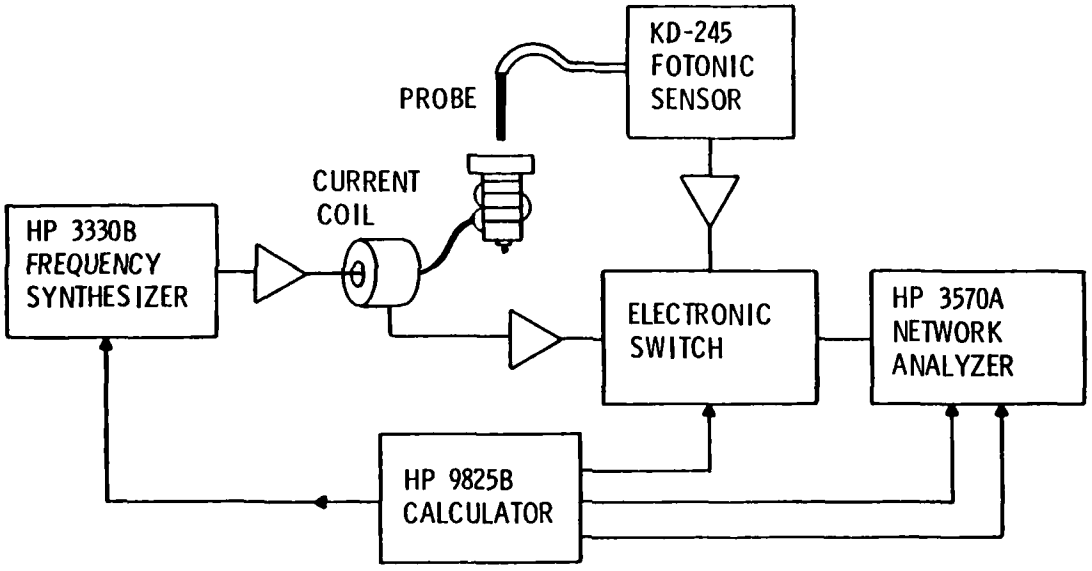

Figure 15. Experimental Set-up for Current-Velocity Measurements

voltage/displacement curve which was matched to the reflectivity of the transducer face. It also clearly showed the probe's range of linear operation.

During measurements, the output voltage from the sensor unit is amplified and filtered. The amplification raises the signal to well above the instrumentation noise floor; the filtering removes both the DC bias arising from the static offset of the probe, and the high frequency leakage from the sensor unit electronics.

If E_d is the displacement voltage measured in dB re .1V, A is the amplification in dB, L_f is the filter loss, S is the sensitivity of the probe in meters/volt, and ω is the radian frequency, then the velocity of the face is

$$U_f = \omega S[10^{(E_d - A + L_f - 20)/20}] \qquad (23)$$

This equation was programmed into the calculator to find the face velocity.

The results of the tests showed that the measurement procedure is repeatable to within ±2 percent. The error comes from the repeatability of the manual positioner calibration. The error could be reduced by designing a more accurate and repeatable positioning system. The velocity proportional and current signals, as displayed on an oscilloscope, were free from noise or distortion. The average value of the transformation factor was .649 Amp-

Sec/Meter; the maximum was .822 and the minimum was .537 A-S/M.

3.4 Frequency Dependence of the Transformation Factor

In order to verify some of the assumptions about the velocity-current technique, a test was conducted to measure the frequency dependence of the measured ϕ values. The calculator was programmed to store the measured velocity and current of a transducer at 200 frequency points over a given range around the transducer's resonance. The results were corrected by using Equation 21, and are shown in Figure 16. Beyond the frequency range shown, the velocity signal becomes significantly degraded by system noise.

The overall non-zero slope of the ϕ curve is probably due to small inaccuracies in the measurement of R in the immittance technique. Since the velocity-current measurement is done near resonance, the $\omega C_o R$ term of Eq. 21 dominates the correction expression. Small changes in R affect the correction term and cause a change in the slope of the ϕ curve. The discrepancies near F_y are probably due to problems in the measurement equipment which could not keep pace with abrupt changes in current and velocity. The Q_m of the transducer in air is high, and, near resonance, the internal transducer parameters are changing too rapidly for the measurement technique programmed into the calculator.

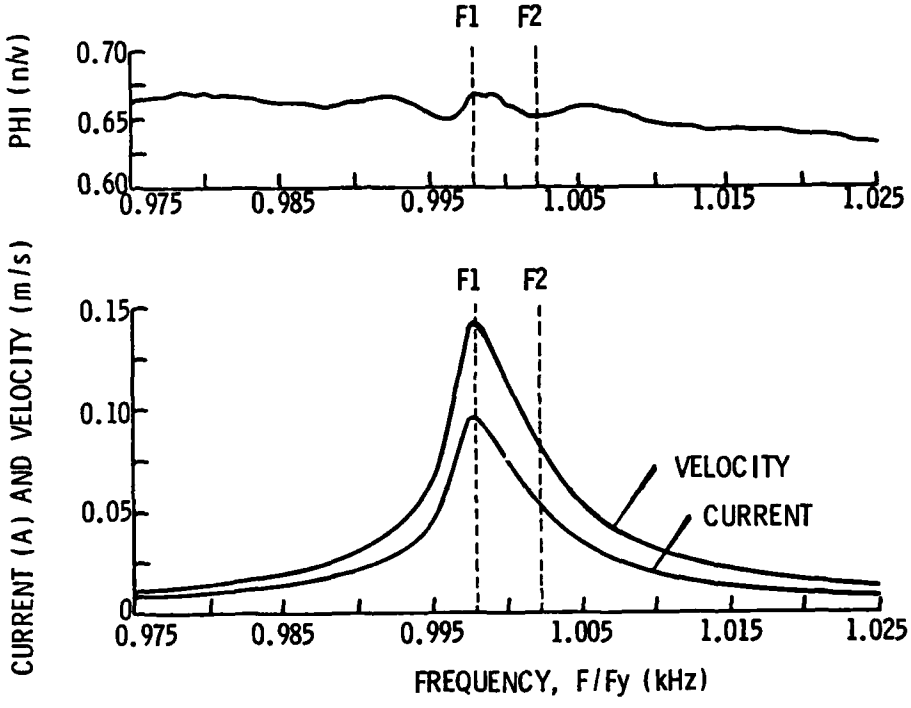

Figure 16. Electromechanical Transformation Factor as a Function of Frequency

Aside from those discrepancies just mentioned, the curve indicates that the electromechanical transformation factor is constant with frequency, as assumed in the derivation of the equivalent circuit model.

CHAPTER 4

APPLICATIONS TO ARRAY PERFORMANCE

4.1 The Inclusion of Radiation Loading

The characteristic responses of a transducer element in water are vastly different than in air: e.g., in water, the resonance frequencies shift, and the quality factor, Q_m, goes down. The changes are caused by the dramatic difference in the radiation loading, or acoustic impedance, between the two media.

The radiation loading may be expressed as follows:

$$Z_a = (\rho c/A)[(R_{self} + R_{mutual}) + j(X_{self} + X_{mutual})] \quad (24)$$

where ρ is the density of the medium, c is the speed of sound in the medium, A is the area of the radiator, R_{self} and X_{self} are the real and imaginary parts of the self impedance, and R_{mutual} and X_{mutual} are the real and imaginary parts of the mutual impedance. If the element is operated singly and not in an array, then R_{mutual} and X_{mutual} are zero.

Taken alone, ρc is called the specific acoustic impedance, with units Kilogram/Meter^2-Second or Rayl. The specific impedances of air and water are 415 and 1.48×10^6 Rayls, respectively. It is this difference in specific

impedance which accounts for most of the variation in transducer performance. Further, the transducers are designed to be operated in water, and the impedance mismatch between the transducer face and the air prevents the transducer from radiating much energy. In air, the mechanical dissipation of R_m is many times greater than the energy radiated into the medium.*

The self impedance is the impedance of the medium to the movement of the transducer face. It is assumed that the face is flush-mounted in an infinite plane rigid baffle. The self impedance terms are functions of the non-dimensional quantity ka, or $\omega a/c$. Thus, the self impedance varies with both the size of the radiator and the frequency.

The mutual interaction impedance is the additional impedance on the transducer face caused by the movement of other transducers nearby. The mutual impedance varies with ka and the relative spacing, orientation, and velocity of the transducers. The total mutual impedance on any element is the sum of contributions from every other element in the array. Generally, because of the symmetry of the array geometry, more than one location in an array may have a given radiation loading. For example, in a five by five

* In the experiments described in the previous chapter, the radiation loading was so low that there was very little difference between air loaded and vacuum (no load) immittance measurements.

array, there are only four unique values of radiation loading, because of the sixfold symmetry of a square array.

More detailed descriptions of the equations and computer programs to find the self and mutual impedance terms are given in Appendices A and B, respectively.

The calculated radiation impedances can be accurately incorporated into the model because of the measurement of the transformation factor ϕ. Without this measurement, it would not be possible to predict the response of an element to the calculated radiation loads. The alternative is to test the transducer elements with water loading, which requires time-consuming bonding techniques. Further, the effects of mutual impedance could only be seen if an entire array were built and tested. This is not desirable, since the goal of the study is to predict array performance before the array is built. The inclusion of radiation loading, using the transformation factor ϕ, is the key to accurate prediction of water-loaded transducer element performance from in-air measurements.

4.2 The Prediction of Array Performance

When the radiation loading for a given array location is incorporated into the lumped-parameter equivalent circuit model of a transducer element, the input/output characteristics of the circuit can be used to predict the

response of the element when it is used in that location. Since the radiation loading varies with location, the response of the element will likewise change with location. This predictive capability can be used to select an optimum transducer element for a given array location.* By combining the predicted responses of every element chosen to be part of a given array, it is possible to predict the response of the entire array, before it is built.

The acoustic performance of an array is judged by four criteria:

1. Transmitting Voltage Response (S_e) in dB re 1 μPa/Volt
2. Transmitting Current Response (S_i) in dB re 1 μPa/Amp
3. Free-Field Voltage Sensitivity (M_e) in dB re 1 Volt/μPa
4. Free-Field Current Sensitivity (M_i) in dB re 1 Amp/μPa

S_e and S_i must also specify the distance at which the measurement is taken. A more detailed explanation of these terms can be found in Albers[9] or in the ANSI standard.[10] These criteria can be derived from the input/output equations for the single transducer element by the following technique.

If an element k in an array is driven with some voltage E, then the volume velocity V_k produced by the element is $|V|_k = |E||T_e|_k$, where $|T_e|_k$ is the response of

* See the next section.

the element as expressed in Equation 5. To find the pressure at a distance r from the array, and hence S_e, the power W_k radiated by the element must be found. This is expressed as $|W|_k = |V|_k^2(R_a)_k$ where $(R_a)_k$ is the real part of the radiation impedance loading on the k^{th} transducer element. The total power W radiated by the array is the sum of the W_k. The total transmitting voltage response of the array, S_e, can be written as

$$S_e = 20\log[\rho cWD/2\pi r^2] \tag{25}$$

where ρ is the density of the medium, c is the sound velocity, and D is the directivity factor of the array. The directivity factor may be expressed as

$$D = 4\pi S/\lambda^2 \tag{26}$$

where S is the area of the array, and λ is the wavelength. By a similar derivation, S_i can be found by using $(T_i)_k$, the transmitting current response of each transducer, as expressed in Equation 7.

The receiving voltage and current sensitivities, M_e and M_i can be found by use of the reciprocity condition,

$$|M_e|/|S_e| = |M_i|/|S_i| = 2r/\rho f \tag{27}$$

M_e and M_i are derived using reciprocity because it is a general measurement practice to connect all of the elements in an array in parallel. Because of this, the

elements interact electrically. Therefore, no simple sum of individual element voltages or current can correctly model the total array voltage or current.

In order to test the prediction technique, the equations for S_e, S_i, M_e, and M_i were programmed into the HP9825B calculator. An array was constructed from the elements selected by the computer routine discussed in the next sections. The measured frequency response of the array was compared to that predicted by the model. The results are shown in Figures 17 through 20. The technique is accurate in predicting the response of the array, within a few dB, over a wide frequency range. Some of the small discrepancy in level and the frequency at which the curve peaks is probably due to the theoretical assumptions used in calculating the radiation impedance. Both the self and mutual impedance were calculated assuming that the radiator was in an infinite baffle, and the actual array was not.

4.3 An Element Selection Method

The Kendig scatter diagram method of element selection, as described in Appendix E, suffers from a number of implementation problems. The derivations for the terms proportional to amplitude and phase are really valid only near F_z. It is also assumed in the derivations that efficiencies and Q_m's do not vary significantly from element to element. Since there was no method for

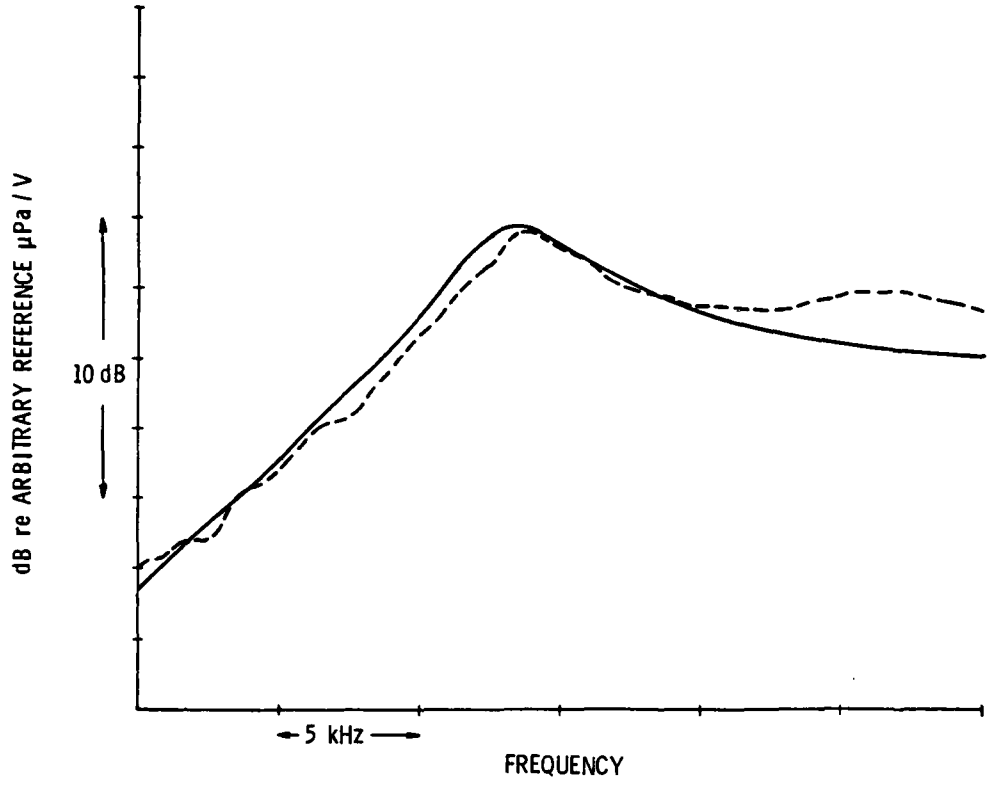

Figure 17. Predicted and Measured S_e

NOTE: Solid lines are predicted values; dashed lines are measured values

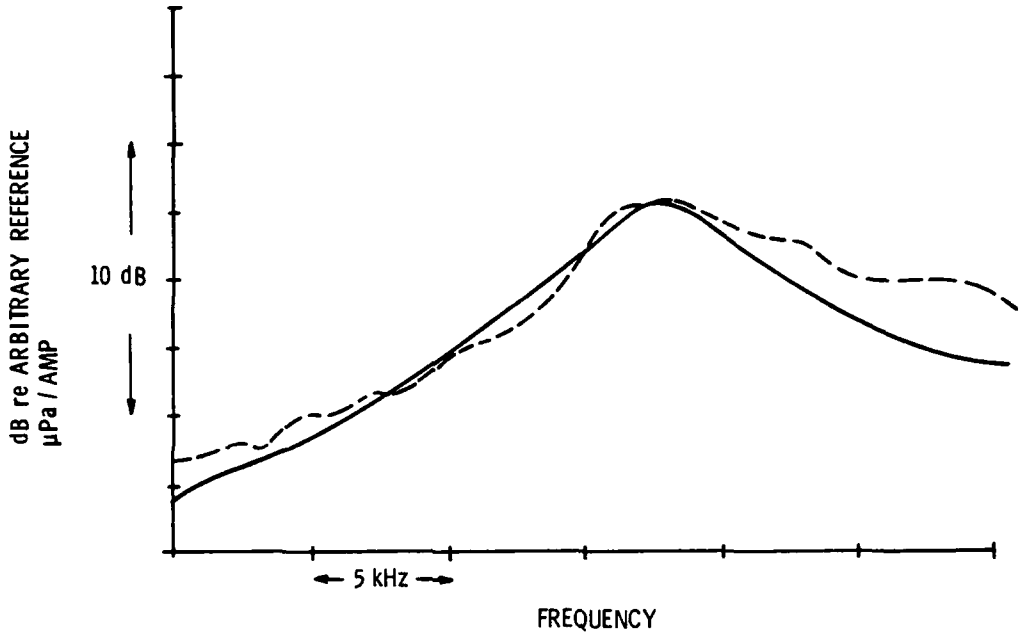

Figure 18. Predicted and Measured S_i

NOTE: Solid lines are predicted values; dashed lines are measured values

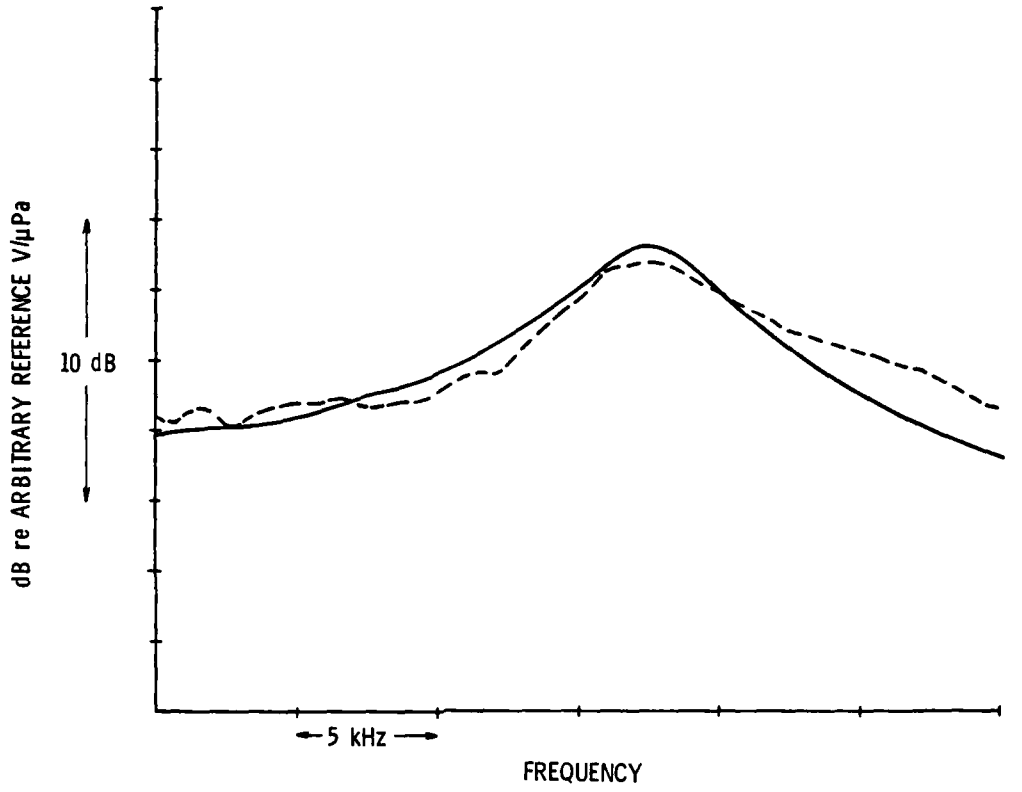

Figure 19. Predicted and Measured M_e

NOTE: Solid lines are predicted values; dashed lines are measured values

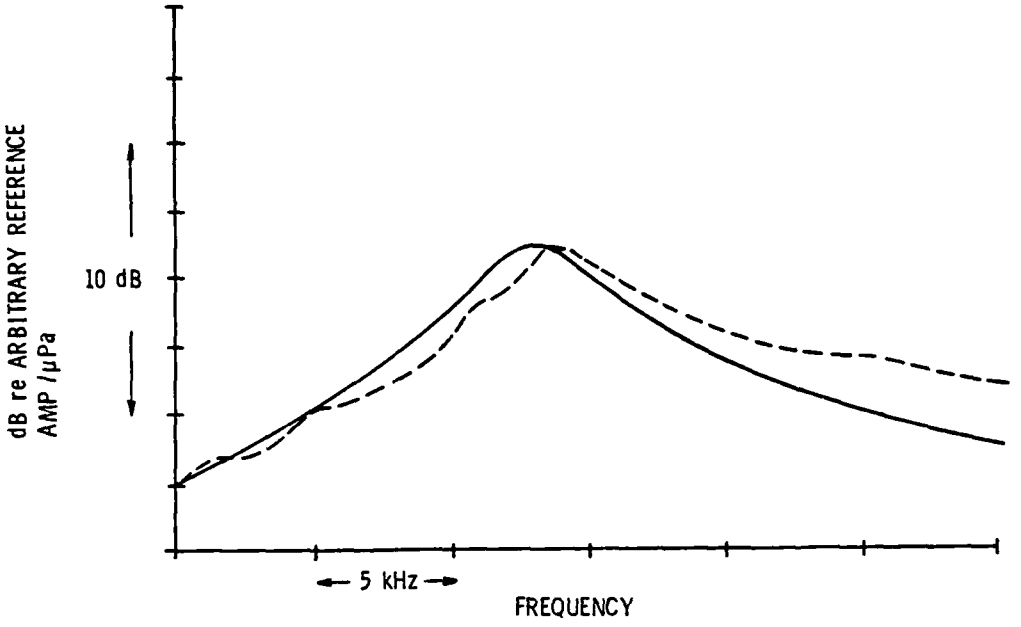

Figure 20. Predicted and Measured M_i

NOTE: Solid lines are predicted values; dashed lines are measured values

accurately measuring the electromechanical transformation ratio, the effect of variations in this parameter had to be ignored. Further, since this factor couples in the effects of radiation impedance , variations in impedance can not be brought into the analysis. It is assumed that the scatter diagram itself will show a Gaussian distribution, which may not be the case for all groups of elements. Finally, it was assumed in the scatter diagram method that equal percentage errors in F_z and $(D_z)^{\frac{1}{2}}$ had equal importance in the selection process. The solutions to many of these problems were beyond the measurement capabilities available at the time. Nonetheless, the technique has been used to construct arrays with performance better than arrays built using a random selection method. However, with the capability to predict the response of a transducer element to any acoustic load, and over a range of frequencies, some of the problems with the Kendig method can be overcome.

The lumped-parameter equivalent circuit model is used as a flexible tool for prediction of element response and is valid over a broad range of frequencies, so that the element selection is not limited to a narrow band around F_z. The actual amplitude and phase of element can be plotted in the scatter diagram, instead of F_z and $(D_z)^{\frac{1}{2}}$. Of particular importance is the effect of acoustic radiation loading on the response of the elements. The acoustic radiation loading plays an important role in

determining an element's position in the scatter diagram. The relative positions of elements within the scatter diagram change with loading. As noted in Appendix B, the variations in acoustic radiation loading caused by mutual interactions fluctuate over a very wide range. The loading varies significantly with both position and frequency.

In order to use the amplitude and phase predictions of the model in a selection method, the predictions must be incorporated into some performance criterion. The Kendig method is essentially a technique for selecting the "best four" elements at a time from the pool of available elements. The four elements are placed into four array locations which are symmetric about the center of the array.* The most central array locations are filled first, and, working outward, the process is repeated until the entire array is filled.

The criteria for "best four" are expressed in terms of position in the scatter diagram. The criteria are closeness to the median amplitude and phase, proximity of paired elements to one another, and opposition of pairs about the median. Underlying the positional criteria is a derivation of the beam pattern response errors due to

* From mutual interaction analysis, it can be shown that, for an unsteered array, four locations symmetric about the array center each have the same total radiation loading. This will become important later in the modelling of the Kendig method.

amplitude and phase variations among the four elements. The positional criteria were derived as a means of minimizing the beam pattern errors. The error derivation forms a better mathematical selection scheme since the relative importance of amplitude and phase deviations tends to be distorted in the scatter diagram.

Of the criteria derived in the Kendig method, one was chosen for the present study. If A_m are the amplitude deviations, and a_m are the phase deviations, then the total error E may be defined as

$$E = A_1a_1 + A_2a_2 + A_3a_3 + A_4a_4 \qquad (28)$$

This error criterion was chosen because of ease of implementation, and because the other criteria either did not involve phase, or were more suited to selecting pairs of elements rather than groups of four. The group of four elements with the lowest value of E was considered the "best four".

The results of using this selection technique versus the Kendig hand-selected method are discussed in the next section.

4.4 A Test Case

The selection and prediction techniques outlined in the previous two sections were tested by using them in the

design of a test array. The array was made up of the elements tested as part of the work described in Chapter Three.

The design goal was to achieve the lowest sidelobe levels possible, using a 42.8 dB shading pattern optimized by a Goal Programming technique.[11] Naturally, this array shading influences the effects of mutual interaction impedance between elements. The variation in element performance, caused by different radiation loadings and element circuit values, results in a distorted array shading pattern and higher than ideal sidelobe levels. It was hoped that the automated selection of elements would result in a design with lower sidelobes than a design using random selection, and possibly with lower sidelobes than a design using the Kendig hand-select method.

The direct implementation of a "best four" approach to the selection process presented a number of problems. First was the sheer size of the combinatorial problem involved in selecting every unique set of four elements from a group of N elements. For N greater than 15, the length of time required to generate and test the combinations becomes excessive. Secondly, it was found that the changes in radiation loading with position caused significant shifts in the amplitude and phase response of the elements. For this reason, the "four best" chosen for

a given set of array locations may not work well with the "best four" for another set of array locations. A method was needed to reduce the number of elements under consideration at one time to less than fifteen and to try to assure that the elements chosen would result in good performance when used all together, and not just as sets of four.

As a solution to the first problem, it was decided to use the average element phase and amplitude as a reference point, and use each element's mean square deviation from this reference as an indication of the element's suitability. Thus an element near the reference was judged better than one further from it. To reduce the number of elements considered at one time, the element with the greatest deviation from the reference point was removed and a new average (reference) computed. This process was repeated until less than fifteen elements remained. Then the combinatorial subroutine selected the "best four" from those remaining. The four elements chosen were stored and removed from further consideration.

In order to reduce the effect of the shifts in amplitude and phase, once the first four elements were chosen, the average amplitude and phase of the four was stored and used as the reference point for all subsequent selections. Thus the process attempted to find the "four

best" elements with respect to the average array amplitude and phase. This improved the uniformity of the element response in the array.

Once an element had been chosen for every position in the array, the resulting beam pattern was predicted. This was done by finding the average amplitude and phase for the entire array, and then expressing the response of each element as a deviation from the average. The ideal response of every location (the shading coefficient) was multiplied by the deviation introduced by the element used at the location. The result is a new array shading pattern, which can be analyzed by standard array beam pattern techniques.*

The selection process as described was implemented on the HP9825B calculator. The program calculated the response of each element for a given acoustic radiation loading, and after eliminating the elements furthest from the reference point, it selected the four which had the lowest value of E. The four were grouped into pairs by matching the two elements with the closest magnitude response. The four elements were printed out and removed from further consideration. The process was repeated, using different radiation loadings, until the array was filled.

* See Appendix F.

In order to gauge the relative effectiveness of the selection technique, two other arrays were designed for comparison. For one array, the Kendig hand-select scatter diagram technique was used. All of the elements were plotted on a scatter diagram, using F_z and $(\dot{D}_z)^{\frac{1}{2}}$ as coordinates. The elements were selected by a person familiar with the method, and the result may be taken as the best selection possible using the hand-select method. Another array was designed by taking the elements selected by the automated technique, and placing them in the array in a random pattern.

The results of the selection routine are shown in Figures 21 through 23. The lines on the graph represent: 1) the ideal beam pattern; 2) the predicted beam pattern for the array designed by the automated technique; 3) the predicted beam pattern for the array design by the Kendig hand-selection method; and 4) the predicted beam pattern for the array of elements selected at random from the automated-design array.

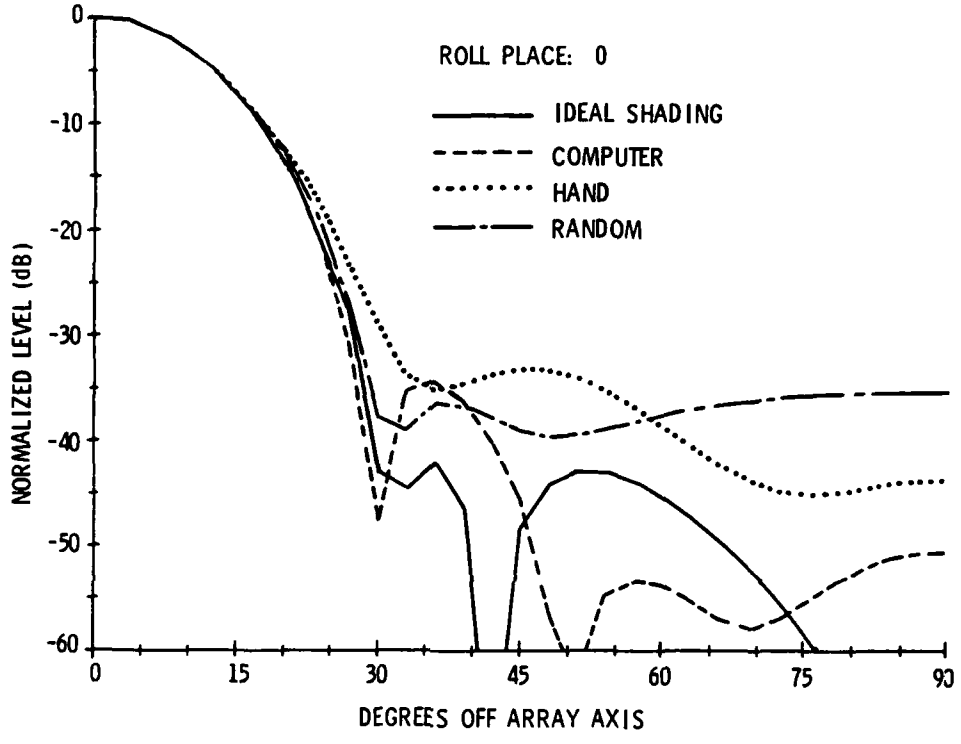

Figure 21. Comparison of Selection Methods: 0° Roll Plane

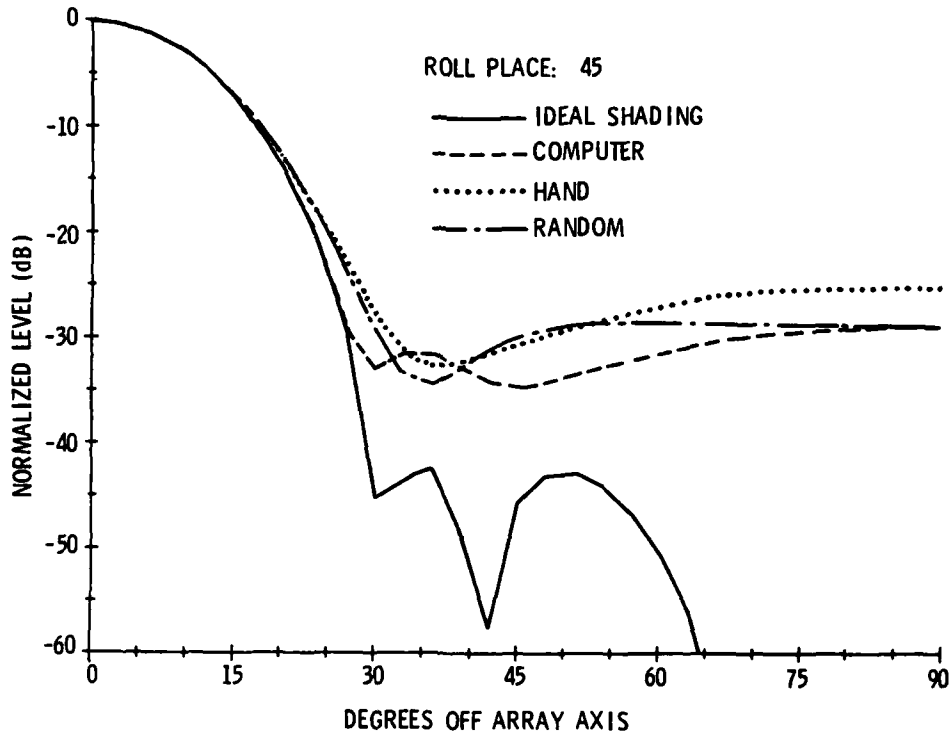

Figure 22. Comparison of Selection Methods: 45° Roll Plane

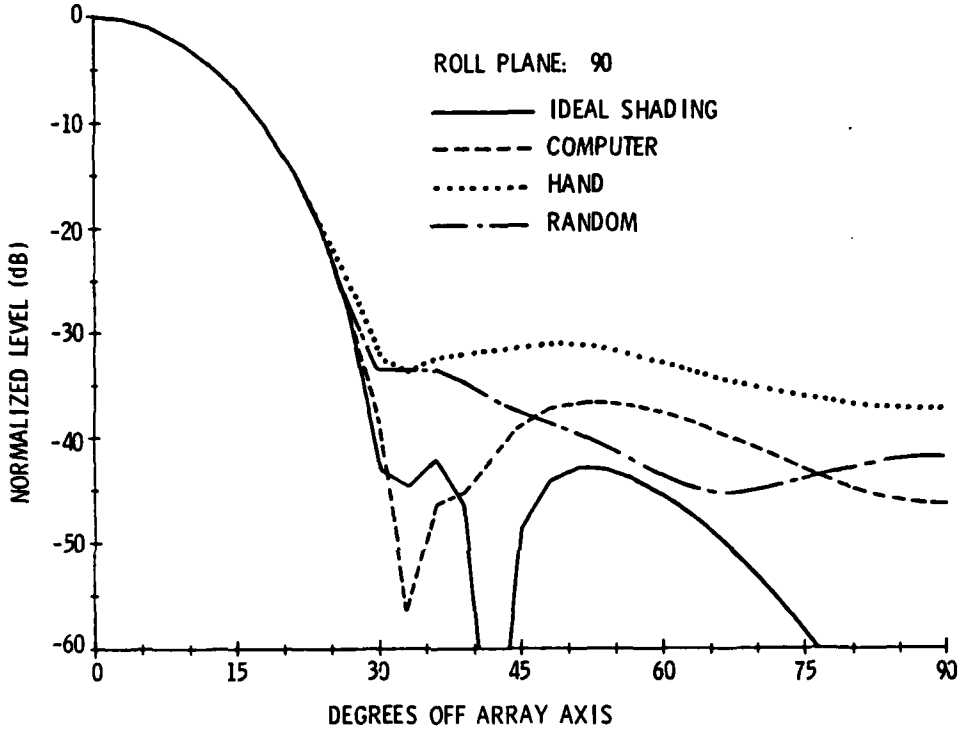

Figure 23. Comparison of Selection Methods: 90° Roll Plane

CHAPTER 5

SUMMARY AND CONCLUSIONS

5.1 Summary

The goal of this thesis was to develop the experimental and computational tools necessary to predict the performance of transducer elements in arrays, using in-air measurements of actual elements. The lumped-parameter equivalent circuit model was used to analyze the characteristics of transducer elements and predict their behavior under varying acoustic loads.

In Chapter 1, the basic problem was presented, and expressed in terms of previous work which had attempted to predict transducer element behavior. The lumped-parameter equivalent circuit model was derived in Chapter 2, and the equations of that chapter form the basis of the measurement and prediction techniques. In Chapter 3, the measurement procedure was developed and implemented. The procedure is completely automated, and is rapid, accurate and repeatable to within $\pm$ 2 percent. The self-check routines built into the programming confirm the accuracy of the equivalent circuit model in predicting transducer immittance over the desired frequency range. The prediction of transducer element performance was presented in Chapter 4. Also

presented in Chapter 4 was a selection technique for placing elements in an array. The directivity pattern of an array designed by the selection technique was compared to patterns of arrays designed by comparable techniques, and showed 5 to 10dB lower sidelobe levels, depending upon the roll plane. The prediction of total array frequency response was within ± 2dB of the measured response of an actual array, over the frequency range of interest.

5.2 Conclusions and Future Studies

The techniques developed in this thesis can be used to significantly improve the array design process, lowering the development cost, reducing the time spent to design hardware, and improving the quality of the final product. Since array performance can be predicted from measurements of just one or two prototype transducer elements, the need to build and test entire prototype arrays is eliminated, dramatically reducing the time and cost involved. With the savings, more effort could be focussed on testing improved designs of transducer elements, since the effect of element changes on array performance could be studied more easily. Also, the selection routine developed has shown promise as a means for automatic selection of transducer element locations within an array.

The accuracy of the predictions could be enhanced, by eithe. uproving the positioning system used in the

velocity measurement, or by attempting to simulate, during the immittance and velocity measurements, the mounting used in array construction.

The techniques as developed, while powerful as a prediction tool, also form a solid basis for further research.

The hardware and software used to measure the electromechanical transformation ratio could easily be modified to study the modal vibration patterns of transducer elements. Using techniques aleady developed, a quantitative study of transducer head flap and its relationship to transducer resonances could be made.

The use of a technique known as Non-Linear Goal Programming or NLGP, as developed by J. P. Ignizio,[12] promises to further improve the element selection techniques derived here. By directly analyzing transducer element choices in terms of predicted beam patterns, NLGP can eliminate most of the problems encountered in modelling the Kendig method, and provide a better final array response.

APPENDIX A

THE ACOUSTICAL IMPEDANCE ON A RECTANGULAR PISTON

The expression for the acoustical radiation impedance is derived in Morse & Ingard.[13] In section 7.4, which deals with radiation from a plane surface, the Green's function is solved to find the reaction force on a rectangular piston with sides of length a and b. The expression is simplified by comparison of series, and for the case of a square piston (a=b), the solution reduces to*

Eq. 7.4.44
$$F_\omega = \rho c u_\omega ab[\theta_o(ka) + jX_o(ka)] \tag{29}$$

where F_ω and u_ω are the force on and velocity of the piston face, and θ_o and X_o are given by

$$\theta_o = 1 - 2J_1(ka)/ka$$

Eq. 7.4.31
$$X_o = M_1(ka) = \frac{4}{\pi}\int_0^{\pi/2} \sin((ka)\cos(q))\sin^2(q)dq \tag{30}$$

J_1 is the first order Bessel function, and M_1 is the first order Struve function.

The computation of J_1 on a large computer is

* This equation has been rewritten to conform to the exponential time dependence convention ($e^{+j\omega t}$) used in this study.

straightforward, since the answer can be obtained through standard scientific subroutine packages. The Struve function requires numerical integration which was done using a three point Gaussian quadrature subroutine.[14] The accuracy of the routine depends upon the number of subintervals taken within the limits of integration. The Struve function converges fairly rapidly, and seven places of accuracy were achieved with little computation time.

These expressions for the radiation loading were implemented in the subroutine RADIMP. The subroutine returns the values of θ_o and X_o for a square radiator used in water, given the length of one side and the frequency of operation. The accuracy of the subroutine was checked by comparing results with Morse and Ingard's Table IX.

The subroutine was used within a larger program which found both the self and mutual impedance for an array of square radiators. The program is listed in Appendix G.

APPENDIX B

THE MUTUAL IMPEDANCE BETWEEN RECTANGULAR PISTONS

The expression for the acoustical mutual interaction impedance between two rectangular pistons is derived by Arase.[15] Figure 24 gives the physical layout of two identical radiators, and the dimensions used in the derivation. If we let

$$\text{Eq. 9} \quad ka = A \qquad kb = B \qquad kg = G \qquad kh = H \tag{31}$$

then the mutual radiation resistance becomes

$$\begin{aligned}\text{Eq. 10} \quad (R_m/\rho cab) = (1/2\pi AB)\{&4C(H,G) - 2C(H-A,G) \\ &- 2C(H,G-B) - 2C(H+A,G) - C(H-A,G+B) \\ &+ C(H+A,G-B) + C(H+A,G+B)\}\end{aligned} \tag{32}$$

where

$$\begin{aligned}\text{Eq. 11} \quad C(x,y) = |x|&\int_{|y|}^{(y^2+x^2)^{1/2}} [(r^2 - y^2)^{1/2}(\cos(r)/r)]dr \\ &+ |y|\int_{|y|}^{(y^2+x^2)^{1/2}} [(r^2 - x^2)^{1/2}(\cos(r)/r)]dr \\ &- \cos(x^2 + y^2)^{1/2} - (x^2 + y^2)^{1/2}\sin(x^2 + y^2)^{1/2}\end{aligned} \tag{33}$$

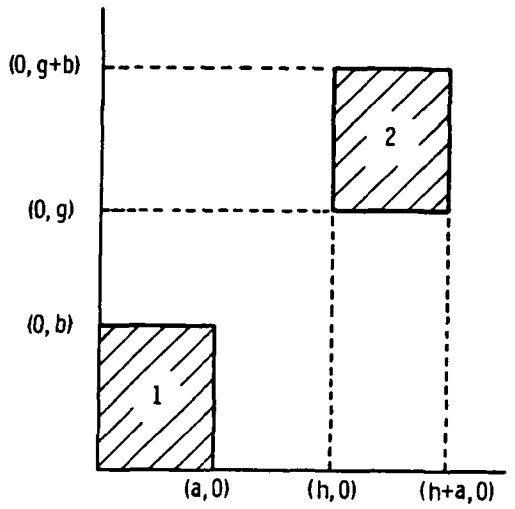

Figure 24. Arrangement and Dimensions of Pistons for Mutual Impedance Calculations

The expression for the mutual radiation reactance X_m divided by ρcab has the same form as Eq. 32, but the function $C(x,y)$ is replaced by $S(x,y)$ in each case, where

$$\text{Eq. 12} \quad S(x,y) = -|x| \int_{|y|}^{(y^2+x^2)^{\frac{1}{2}}} [(r^2 - x^2)^{\frac{1}{2}}(\sin(r)/r)]dr - |y| \int_{|y|}^{(y^2+x^2)^{\frac{1}{2}}} [(r^2 - x^2)^{\frac{1}{2}}(\sin(r)/r)]dr$$

$$- (x^2 + y^2)^{\frac{1}{2}}\cos(x^2 + y^2)^{\frac{1}{2}} + \sin(x^2 + y^2)^{\frac{1}{2}} \qquad (34)$$

The computation of R_m and X_m involved the numerical integration of Eqs. 33 and 34, using the same three point Gaussian quadrature routine discussed in Appendix A. The listing of the program to find the total loading on an 8 X 8 array of elements is given in Appendix G.

The total mutual interaction impedance on an element in an array is the weighted sum of the contributions from every other element in the array. If $Z_m^{j,k}$ is the impedance on the j^{th} element due to the movement of the k^{th} element, then the total loading on the j^{th} element in an array of M elements is

$$Z_m^j = \sum_{k=1}^{M} (U_k/U_j)Z_m^{j,k} \qquad (35)$$

where U_k and U_j are the velocities of the k^{th} and j^{th} elements respectively, and $Z_m = R_m + jX_m$. If we label the self impedance on the element, as found in the previous Appendix, as Z_s^j, then the total loading on the j^{th} element is

$$Z_{total}^j = Z_s^j + \sum_{\substack{k=1 \\ k\neq j}}^{M} (U_k/U_j) Z_m^{j,k} \qquad (36)$$

From this it is evident that the loading on an element wil vary with: 1) position in the array, and 2) the array shading distribution, which affects the relative velocities of the elements. For the case of an 8 X 8 array, as shown in Figure 25, there are ten unique values of radiation loading, due to the symmetry of the array. The letters A through J denote those positions.

To illustrate the first point, the variation of loading with position and frequency is shown for locations A, D, and H in Figures 26 and 27. Figure 26 is for the real part of the loading; Figure 27 is for the imaginary part of the loading. The solid line is the loading on a single element and the line on the frequency axis denotes the frequency for which $k = \pi$. It is easily seen that the loading varies significantly with position and frequency, especially below $k = \pi$.

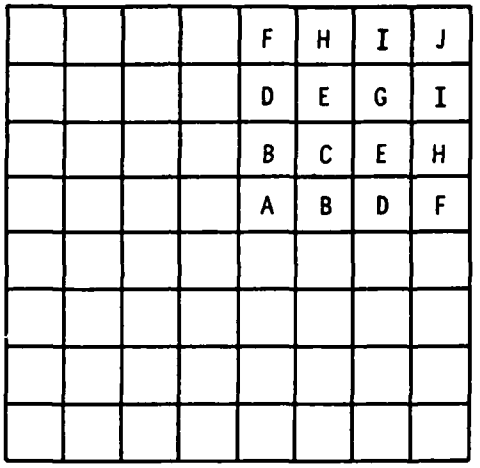

Figure 25. 8 X 8 Array Positions

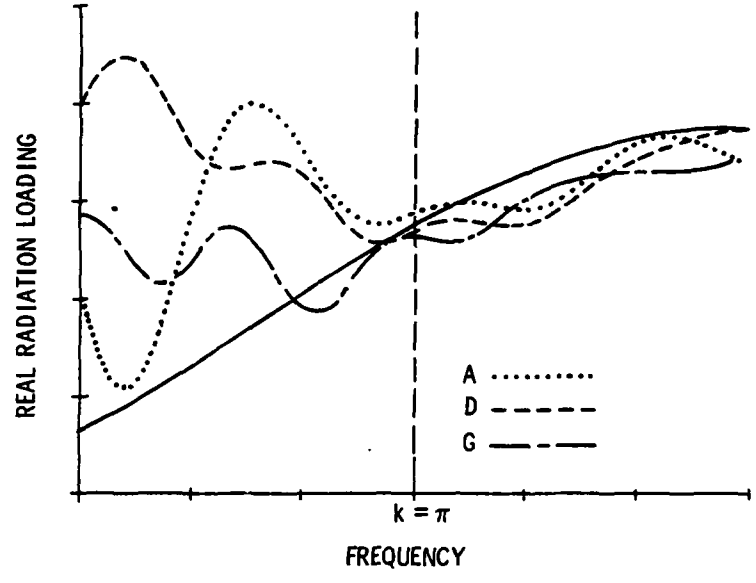

Figure 26. Comparison of Real Radiation Loading for Three Array Positions

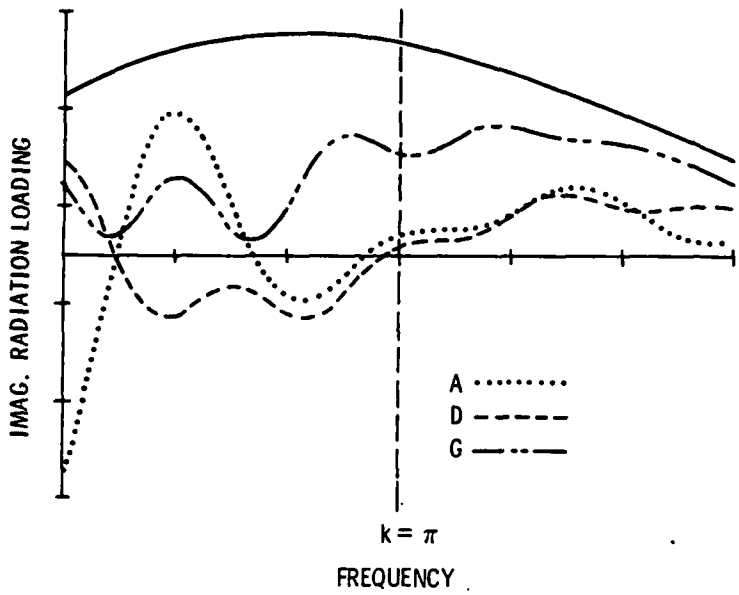

Figure 27. Comparison of Imaginary Radiation Loading for Three Array Positions

Table 1 demonstrates the variation in loading caused by changing the array shading. The values in the table have been normalized by the loading on a single element. The frequency used for this example was chosen such that $k = \pi$.

TABLE 1

Comparison of Radiation Loading by Position

For Various Shading Patterns

POSITION	LOADING*	UNSHADED	SHADING 1	SHADING 2
A	REAL	1.041	1.082	1.082
	IMAG	0.063	0.126	0.131
D	REAL	0.975	1.077	1.095
	IMAG	0.017	0.105	0.106
E	REAL	1.232	1.130	1.122
	IMAG	-0.033	0.097	0.093
F	REAL	1.176	1.157	1.161
	IMAG	0.282	1.372	0.055
H	REAL	0.970	1.046	1.124
	IMAG	0.370	0.057	-0.057

POSITION SHADING COEFFICIENTS FOR SHADING 1

A: 1.0	B: 0.7606	C: 0.5844	D: 0.4672	E: 0.3561
F: 0.1882	G: 0.2196	H: 0.1186	I: 0.0102	J: 0.0015

POSITION SHADING COEFFICIENTS FOR SHADING 2

A: 1.0	B: 0.7282	C: 0.5263	D: 0.3815	E: 0.2632
F: 0.1095	G: 0.1189	H: 0.0612	I: 0.0131	J: 0.0014

*NOTE: The radiation loadings have been scaled as explained in the text.

APPENDIX C

USING THE HP3750 TO MEASURE IMMITTANCE

The HP3570 Network Analyzer is designed to measure the transfer function response of two-port networks. However, with the use of special input terminations and simple formulae, the analyzer can be used to find the input immittance of one-port devices.

The standard mode of operation of the analyzer is shown in Figure 28. The analyzer supplies a voltage V to two output terminals A_{out} and B_{out}, which are connected to the inputs of the networks under test. Generally, one network, fed by A_{out}, is used as a reference or standard, and the network fed by B_{out} is to be compared with the reference. The outputs of the reference and test networks are connected into A_{in} and B_{in}, respectively. The analyzer measures A_{in} and B_{in}, and finds the ratio $E = |A_{in}|/|B_{in}|$ and the phase angle $P = Arg(A_{in}) - Arg(B_{in})$. The resistors marked R_{int} are the internal source impedance of the driving voltage sources, and the resistors marked R_{ext} are external resistors used for impedance matching.

To use the analyzer for immittance measurements, the set-up shown in Figure 29 is used. The A channel is

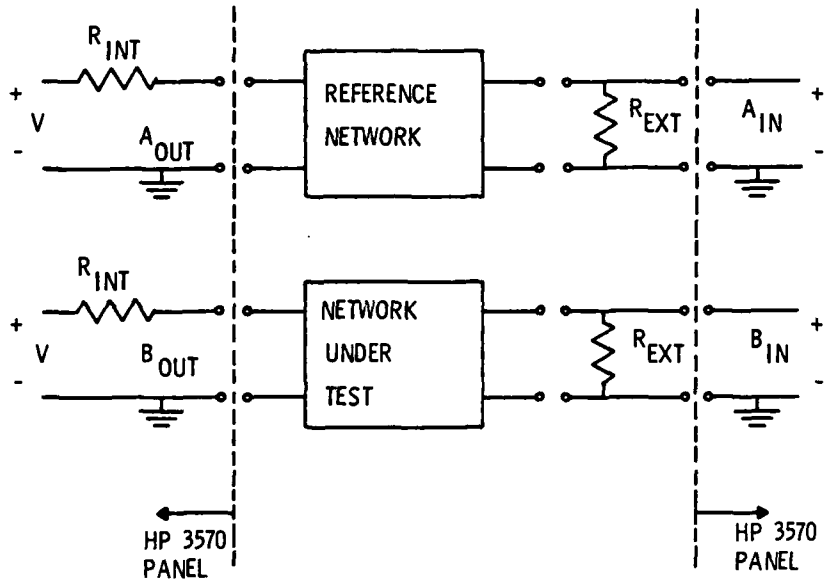

Figure 28. Standard HP3570 Set-up

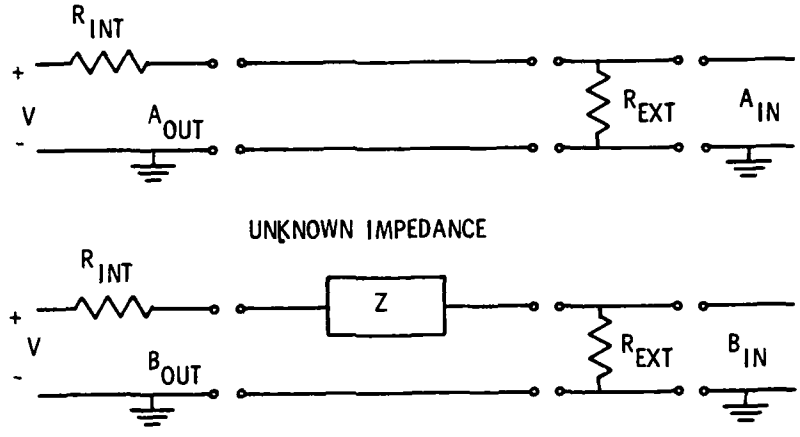

Figure 29. HP3570 Set-up for Immittance Measurements

shorted, except for the matching resistor R_{ext}, and the B channel is connected to the unknown impedance Z, again with the matching resistor.

The equivalent circuits for the equipment set-up in Figure 29 are shown in Figure 30. Solving for A_{in} and B_{in},

$$A_{in} = V\{R_{ext}/(R_{int} + R_{ext})\}$$

$$B_{in} = V\{R_{ext}/(R_{int} + R_{ext} + Z)\} \quad (37)$$

Since the unknown impedance can be both resistive and reactive, let $Z = \mathcal{R} + jX$. Substituting into the above and solving for E and P yields

$$E = \{[(R_{int} + R_{ext} + R)^2 + X^2]\}^{\frac{1}{2}}/(R_{int} + R_{ext})\}$$

$$P = \tan^{-1}\{X/(R_{int} + R_{ext} + R)\} \quad (38)$$

These two equations can be solved for R and X, which yields

$$R = (R_{int} + R_{ext})[E\cos(P) - 1]$$

$$X = (R_{int} + R_{ext})E\sin(P) \quad (39)$$

For the experiments described in Sections 3.1 and 3.2, the resistors R_{int} and R_{ext} were equal to 75 Ohms. Therefore

$$R = 150[E\cos(P) - 1] \quad X = 150E\sin(P) \quad (40)$$

AD-A114 816 PENNSYLVANIA STATE UNIV UNIVERSITY PARK APPLIED RESE--ETC F/G 9/1
THE PREDICTION OF TRANSDUCER ELEMENT PERFORMANCE FROM IN-AIR ME--ETC(U)
JAN 82 M E SCHAFER N00024-79-C-6043
UNCLASSIFIED ARL/PSU/TM-82-62 NL

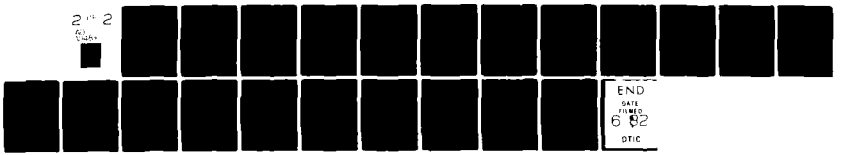

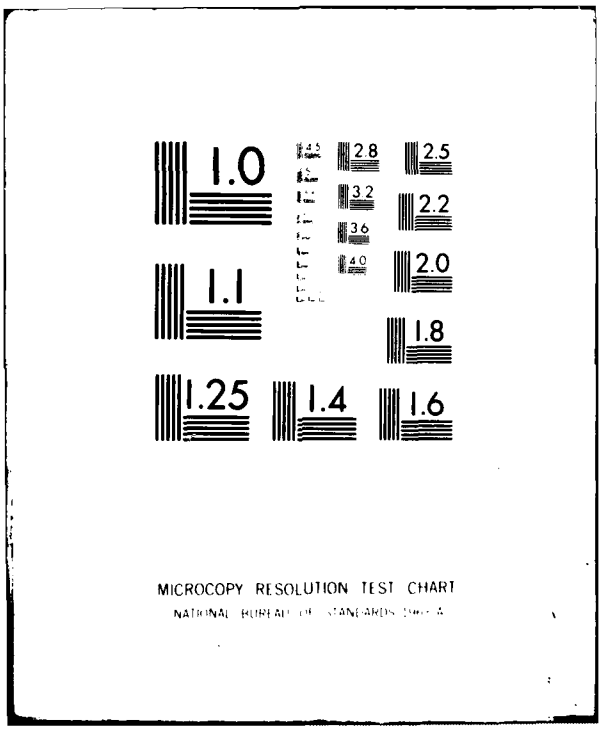
1.0
1.1
1.25
1.4
1.6
1.8
2.0
2.2
2.5
2.8
3.2
3.6
4.0
MICROCOPY RESOLUTION TEST CHART
NATIONAL BUREAU OF STANDARDS 1963-A

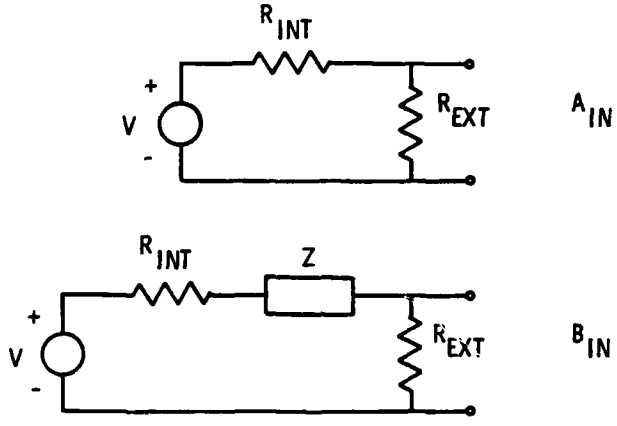

Figure 30. Equivalent Circuit for HP3570 Immittance Measurements

Solving for the admittance yields

$$G = (\cos(P)E - 1)/\{150[E^2 - 2\cos(P)E + 1]^{\frac{1}{2}}\}$$

$$B = \sin(P)E/\{150[E^2 - 2\cos(P)E + 1]^{\frac{1}{2}}\} \quad (41)$$

These last two sets of equations were programmed into the HP9825B calculator to find the immittance of the transducer elements.

APPENDIX D

THE INFLUENCE OF R_o ON THE EQUIVALENT CIRCUIT

In order to assess the influence of R_o on the equivalent circuit, the following method was used to estimate R_o from the measurements described in Section 3.1.

From Figure 13, it was assumed that the difference between the measured and predicted impedance peaks at $_z$ was due to neglecting R_o in the equivalent circuit. Figure 31 shows how R_o would affect the equivalent circuit. If R_z is the predicted resistance of the equivalent circuit evaluated at ω_z, then R_z' would be lower than R_z, depending upon the value of R_o. If R_z' were set to the measured resistance of the transducer element at ω_z, then the circuit can be solved to find R_o. Solving for R_o yields

$$R_o|_{\omega_z} = (R_z R_z')/(R_z' - R_z) \qquad (42)$$

R_o varies inversely with frequency, and the [illegible]nce is more properly expressed as $R_o = (R_o'/\omega)$, where R_o' i[illegible]e theoretical DC resistance. Multiplying the value of R_o found using Eq. 42 by ω_z gives an estimate of R_o'.

For the transducer elements measured in this study, the values of R_o' found in this manner ranged between

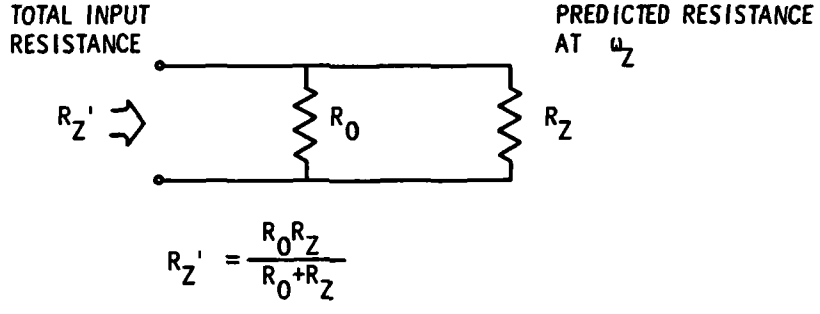

Figure 31. Effect of Adding R_o to the Equivalent Circuit

1.5 and 3.0 X 10^{11} Ohms. When this was put into the proper equivalent circuit expressions, the difference in transmit and receive levels did not vary more than .1 dB. Therefore, it was concluded that, for the transducer elements tested, the ommission of R_o did not significantly affect the final results.

APPENDIX E

THE KENDIG SCATTER DIAGRAM SELECTION METHOD

In his report, (Ref. [1]), Kendig describes a method for reducing the detrimental effects of non-ideal elements on array performance. He developed a selection method for the placement of elements within an array, based upon their relative amplitude and phase response. The first part of his report is a derivation of the parameters needed for prediction of element response; the second part is a description of a selection scheme for choosing element positions in an array to reduce minor lobe levels.

Kendig shows that, near F_z, the free field voltage sensitivity M_o is approximately proportional to (ηD_z), where η is the efficiency of the element, and

$$D_z = k_{eff}^2 Q_z / F_z (C + C_o)(1 - k_{eff}^2) \qquad (43)$$

where Q_z is the mechanical quality factor of the water-loaded transducer. The values of F_z, k_{eff}^2, and $(C + C_o)$ are measured using techniques similar to those discussed in Section 3.1. Since it was not practical to measure the efficiency and Q_m of every transducer, it was assumed that these parameters did not vary significantly from element to element. In another report,[16] Kendig had shown that phase

errors in hydrophone elements were proportional to F_z, assuming that the positioning of the elements in the array could be held to close tolerance. Thus, by comparing the values of F_z and $(D_z)^{\frac{1}{2}}$, a relative measure of transducer element amplitude and phase could be made from in-air measurement procedures. The comparison was made graphically in the form of a scatter diagram, such as Figure 32. Each point represents a transducer element; the X represents the median combination of F_z and $(D_z)^{\frac{1}{2}}$. Kendig assumed that the distribution of amplitude and phase errors would follow a Gaussian distribution. The closeness of an element to the median gives an indication of the relative magnitue of amplitude and phase errors.

Next, Kendig described the effect of amplitude and phase errors on array performance. Figure 33 represents two pairs of array elements which are symmetrically spaced about the array center. If A_n is the amplitude, and a_n is the phase error of an element, then the contribution of these four elements to the horizontal array pattern may be expressed as

$$P_{(real)} \approx [(A_1+A_2) + (A_3+A_4)]\cos(nu) - [(A_1a_1-A_3a_3) - (A_2a_2-A_4a_4)]\sin(nu) \quad (44)$$

$$P_{(imag)} \approx [(A_1-A_3) + (A_2-A_4)]\sin(nu) + [(A_1a_1+A_3a_3) + (A_2a_2+A_4a_4)]\cos(nu) \quad (45)$$

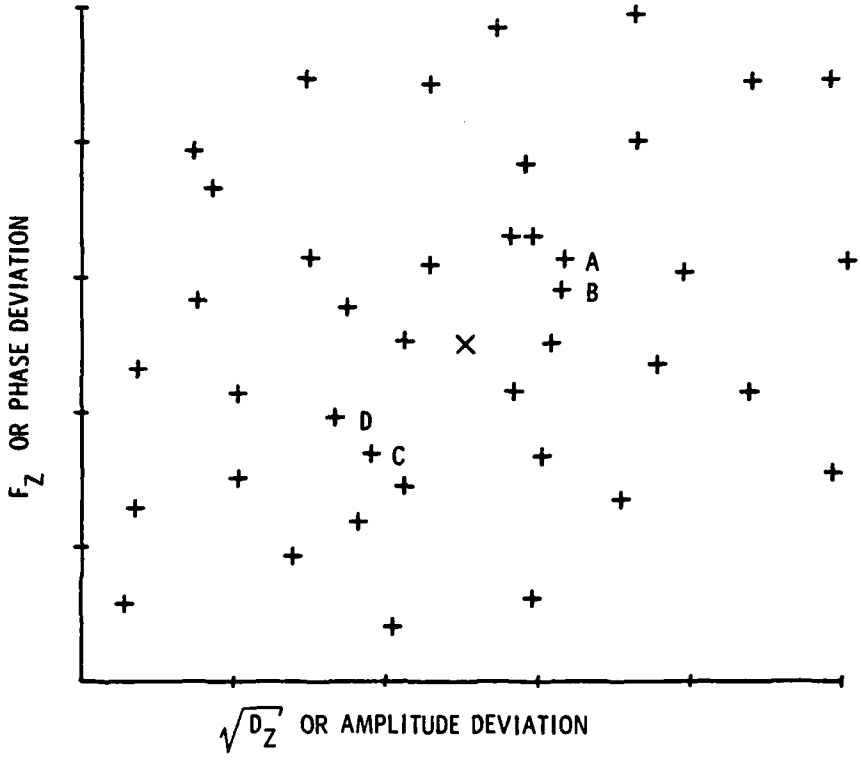

Figure 32. Scatter Diagram from Kendig[1]

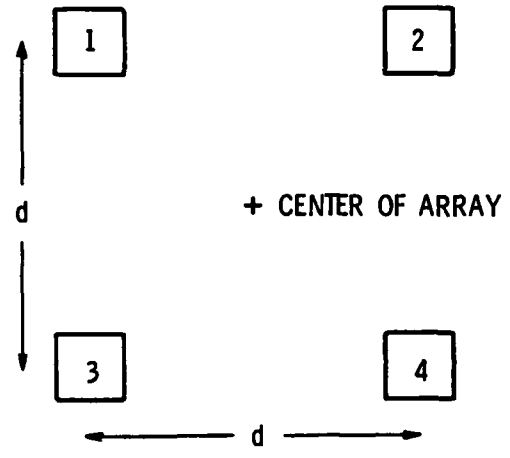

Figure 33. Four Symmetric Array Locations from Kendig[1]

where n is an integer, u is equal to $d\omega\sin(\theta)/2c$, d is the element spacing, and θ is the incident angle. In the ideal case, all of the A_ns are equal, and all of the a_ns are zero. The terms in the above equations are grouped to show the offsetting contributions from specific pairs within the group of four. It is desired that both the second term of Eq. 44 and all of Eq. 45 be equal to zero. Further, the first term of Eq. 44 should be equal to four times the median element amplitude.

Applying the two equations above to the scatter diagram, Kendig proposed the following selection process: pick two elements which are close to one another in the scatter diagram, such as A and B, and place them in positions 1 and 3. By doing this, the $(A_1a_1-A_3a_3)$ and (A_1-A_3) terms are made small. Elements C and D are then chosen for positions 2 and 4. These two elements are also close together in the scatter diagram, which makes $(A_2a_2-A_4a_4)$ and (A_2-A_4) small. Further, since C and D are nearly opposite in amplitude and phase error from A and B, the second term of Eq. 45 will be small, and the first term of Eq. 44 will be nearly equal to four times the median element amplitude.

APPENDIX F

ARRAY BEAM PATTERN RESPONSE

The beam pattern response of an array is the sum of the contributions from all of the elements within the array. The following derivation is for a planar array of point elements, but is can easily be extended to find the response of an array of square radiators.

Consider a point element m in a plane array located at position (x_m, y_m), as shown in Figure 34. For a wave coming from the (θ, ϕ) direction, the contribution of the m^{th} element to the total array signal is

$$Q_m = A_m e^{j(\omega t + u)}$$

$$= A_m e^{j\omega t}[(\cos(u) + j\sin(u)] \qquad (46)$$

where

$$u = kx_m \sin\theta\cos\phi + ky_m \sin\phi\sin\phi + a_m$$

and A_m is the element amplitude shading and a_m is the element phasing. The $e^{j\omega t}$ time dependence may be dropped, since it is common to all the elements, and therefore does not contribute any information to the directional response. The total response of the array of M elements is simply the sum of the contributions of each element.

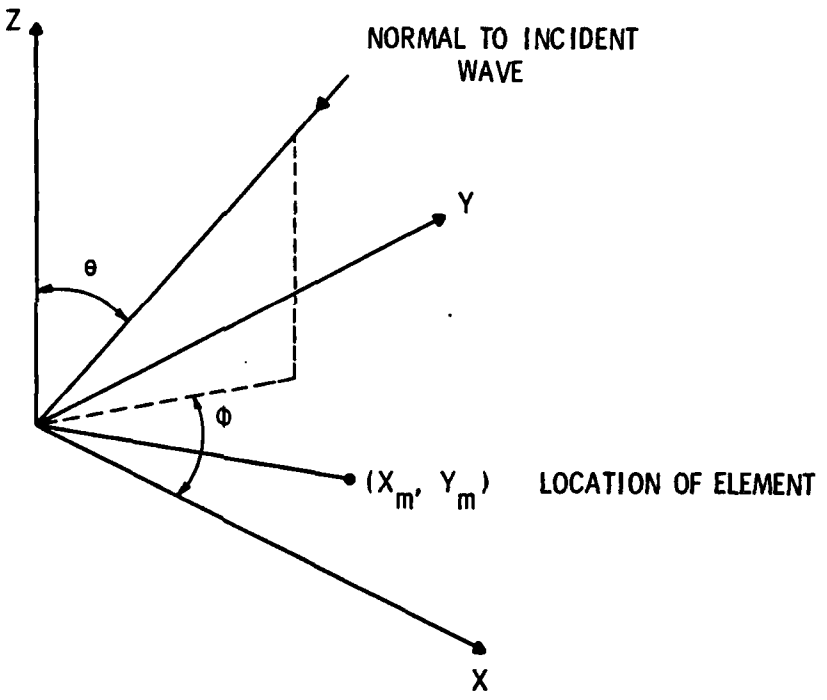

Figure 34. Coordinate System for Beam Pattern Response Derivation (after Draus[11])

$$Q_{tot} = \sum_{m=1}^{M} A_m\{\cos[kx_m \sin\theta\cos\phi + ky_m \sin\theta\sin\phi + a_m] + j\sin[kx_m \sin\theta\cos\phi + ky_m \sin\theta\sin\phi + a_m]\} \quad (47)$$

The subroutine PRESS was used to implement Eq. 47, returning the array amplitude and phase for any direction. For the beam pattern predictions described in Section 4.3, each ideal A_m and a_m was modified to include the error introduced by the m^{th} element.

For an array of square elements of side C, the directivity of the elements must be included in Eq. 47. This is done by modifying A_m:

$$A_m' = A_m\{[\sin(.5kC|\sin\theta\sin\phi|)/(.5kC|\sin\theta\cos\phi|)] \times [\sin(.5kC|\sin\theta\cos\phi|)/(.5kC|\sin\theta\cos\phi|)]\} \quad (48)$$

A listing of the subroutine PRESS follows.

```
      SUBROUTINE PRESS(THETAP,PHIP,AMPL,PHASE)
C ***********************************************************
C
C              SUBROUTINE TO FIND ARRAY RESPONSE
C
C  RETURNS  AMPLITUDE AND PHASE (DEG) RESPONSE OF AN ARRAY.
C
C INPUTS ARE BEAM ANGLE THETA AND ROLL PLANE PHI(DEGREES).
C ELEMENT LOCATIONS ARE IN ARRAYS X AND Y;
C ELEMENT SHADINGS ARE IN THE COMPLEX ARRAY ELEMNT,
C STORED IN THE THE FORM OF MAGNITUDE AND PHASE (DEG).
C AK IS THE WAVENUMBER (K) AND M IS THE NUMBER OF ELEMENTS.
C
C ***********************************************************
      COMMON X(101),Y(101),ELEMNT(101),AK,M
      REAL*4 ANGLE(101),A(101)
      REAL*8 U,SUMR,SUMI,DCOS,DSIN,DATAN2,DAMPL
      COMPLEX ELEMNT
C CONSTANTS TO CONVERT DEGREES TO RADIANS AND VICE VERSA
      DATA RAD2D/57.2958/,D2RAD/1.74532925 E-02/
C INITIALIZE SUMS AND SET ANGLE PARAMENTER
      SUMR = SUMI = 0.0
      UCOS=SIN(THETAP*D2RAD)*COS(PHIP*D2RAD)
      USIN=SIN(THETAP*D2RAD)*SIN(PHIP*D2RAD)
C SUM OVER ELEMENTS
      DO 10 J=1,M
      A(J)=REAL(ELEMNT(J))
      ANGLE(J)=AIMAG(ELEMNT(J))
      U=DBLE(AK*X(J)*UCOS+AK*Y(J)*USIN+ANGLE(J)*D2RAD)
      DAMPL=DBLE(A(J))
      SUMR=SUMR+DCOS(U)*DAMPL
  10  SUMI=SUMI+DSIN(U)*DAMPL
C TAKE MAGNITUDE OF AMPLITUDE AND PUT PHASE IN DEGREES
      AMPL=SNGL(SUMR*SUMR+SUMI*SUMI)
      AMPL=SQRT(AMPL)
      PHASE=SNGL(DATAN2(SUMI,SUMR))*RAD2D
      RETURN
      END
```

APPENDIX G

LISTING OF THE RADIATION IMPEDANCE PROGRAM

The following program was used to find the total radiation loading on the array of elements.

```
C PROGRAM TO FIND THE TOTAL LOADING ON THE
C    UNIQUE ARRAY POSITIONS IN AN 8X8 ARRAY.
C    THE RADIATION LOADING IS THE COMBINATION
C    OF THE SELF IMPEDANCE, FOUND IS SUBROUTINE
C    RADIMP, AND THE MUTUAL INTERACTION IMPEDANCE,
C    FOUND IN SUBROUTINE MUTRAD.
C    THE MUTUAL IMPEDANCE COEFFICIENTS ARE GENERATED
C    BY SUBROUTINE FINDMT.
C    THE OUTPUT VARIES DEPENDING UPON THE SHADING PATTERN.
C    THE INPUTS TO THE PROGRAM ARE THE LENGTH OF THE
C    SIDE OF AN (SQUARE) ELEMENT, AND THE STARTING
C    FREQUENCY, THE NUMBER OF FREQUENCY STEPS AND
C    THE SIZE OF THE FREQUENCY STEPS.
      IMPLICIT REAL*8 (E,M,X,Y,V)
      REAL*8 ELEMNT(52,3),MUTARA(35,4),FREQ(21),LENGTH
      REAL*8 DKA,RM,XM,RMUTOT,XMUTOT,RTOT,XTOT,VELRAT
      REAL*8 UNIPOS(8,3),LOAD(21,9,3)
      DIMENSION ARAPOS(8),M1(4),M2(4)
C     SETTING UP ARRAY
      COMMON/MUTUAL/MUTARA
      DATA M1/1.,-1.,1.,-1./
      DATA M2/1.,1.,-1.,-1./
      DATA(UNIPOS(J,1),J=1,8)/0.5D0,2*1.5D0,2*2.5D0,
         3.5D0,2.5D0,3.5D0/
      DATA(UNIPOS(J,2),J=1,8)/2*.5D+0,1.5D+0,.5D+0,1.5D+0
     1,.5D+0,2.5D+0,1.5D+0/
      DATA(UNIPOS(J,3),J=1,8)/8*1.0D+0/
      DATA (ARAPOS(J),J=1,8)/1HA,1HB,1HC,1HD,1HE,1HF,1HG,1HH/
      K=0
      DO 27 J=1,8
      DO 25 N=1,4
      K=K+1
      ELEMNT(K,1)=M1(N)*UNIPOS(J,1)
      ELEMNT(K,2)=M2(N)*UNIPOS(J,2)
      ELEMNT(K,3)=UNIPOS(J,3)
      IF(UNIPOS(J,1).EQ.UNIPOS(J,2)) GO TO 25
      K=K+1
      ELEMNT(K,1)=M1(N)*UNIPOS(J,2)
      ELEMNT(K,2)=M2(N)*UNIPOS(J,1)
      ELEMNT(K,3)=UNIPOS(J,3)
   25 CONTINUE
   27 CONTINUE
```

```
C     ENTER LENGTH, STARTING FREQ., FREQ. STEP SIZE, AND
C     NUMBER OF STEPS
      READ(5,110) LENGTH
      READ(5,111)STRTFQ,STEPFQ,NUMSTP
      DO 30 N = 1,NUMSTP
      FREQ(N) = STRTFQ + STEPFQ*FLOAT(N-1)
C     FIND SELF IMPEDANCE, AND FILL MUTUAL IMPEDANCE ARRAY
      CALL RADIMP(FREQ(N),LENGTH,RM,XM)
      CALL FINDMT(FREQ(N),LENGTH)
C     SELF IMPEDANCE IS IN THE FIRST OUTPUT ARRAY POSITION
      LOAD(N,1,1) = (.15D+04)*(.1026D+04)*RM/(LENGTH**2.)
      LOAD(N,1,2) = (.15D+04)*(.1026D+04)*XM/(LENGTH**2.)
C     SUM MUTUAL IMPEDANCES OVER ALL ELEMENTS
      DO 20 L=1,8
      RMUTOT = 0.0D+00
      XMUTOT = 0.0D+00
      DO 15 K=1,52
      IF(ELEMNT(K,1).EQ.UNIPOS(L,1).AND.
     1ELEMNT(K,2).EQ.UNIPOS(L,2)) GO TO 15
      XDIFF = DABS(UNIPOS(L,1)-ELEMNT(K,1))
      YDIFF = DABS(UNIPOS(L,2)-ELEMNT(K,2))
      VELRAT = ELEMNT(K,3)/UNIPOS(L,3)
      CALL MUTRAD(XDIFF,YDIFF,RMUT,XMUT)
      RMUTOT = RMUTOT + VELRAT*RMUT
      XMUTOT = XMUTOT + VELRAT*XMUT
   15 CONTINUE
C     ADD SELF AND MUTUAL IMPEDANCES
      RTOT = RMUTOT + RM
      XTOT = XMUTOT + XM
      LOAD(N,L+1,1) = (.15D+04)*(.1026D+04)*RTOT/(LENGTH**2.)
      LOAD(N,L+1,2) = (.15D+04)*(.1026D+04)*XTOT/(LENGTH**2.)
   20 CONTINUE
   30 CONTINUE
      WRITE(6,113)
      WRITE(6,114)
      WRITE(6,115)
      WRITE(6,116)(ARAPOS(J),J=1,8)
      DO 40 N=1,21
      WRITE(6,120)IDINT(FREQ(N)),(LOAD(N,J,1),J=1,9)
      WRITE(6,121)(LOAD(N,J,2),J=1,9)
  110 FORMAT(F10.6)
  111 FORMAT(2F10.2,I2)
  113 FORMAT(5X,' ',///)
  114 FORMAT(51X,'P O S I T I O N  I N  T H E  A R R A Y')
  115 FORMAT(13X,'SINGLE')
  116 FORMAT(1X,'FREQUENCY',3X,'ELEMENT',8X,A1,7(11X,A1),/)
  117 FORMAT(1X,'FREQUENCY',18X,A1,7(11X,A1),////)
  120 FORMAT(3X,I5,1X,9(3X,D9.3))
  121 FORMAT(9X,9(3X,D9.3),/)
   40 CONTINUE
      WRITE(6,117)(ARAPOS(J),J=1,8)
      STOP
      END
C SUBROUTINE TO FIND THE MUTUAL INTERACTION IMPEDANCE
```

```
C    COEFFICIENT BETWEEN THE REFERENCE ELEMENT AND THE
C    ELEMENT AT THE POSITION PASSED TO THE SUBROUTINE.
       SUBROUTINE MUTRAD(XDIFF,YDIFF,RMUT,XMUT)
       IMPLICIT REAL*8 (E,M,X,Y,V)
       REAL*8 MUTARA(35,4)
       COMMON/MUTUAL/MUTARA
       DO 10  K=1,35
       IF((DABS(MUTARA(K,1)-XDIFF).LE.0.1D-03.AND.
      1DABS(MUTARA(K,2)-YDIFF).LE.0.1D-3).OR.
      2(DABS(MUTARA(K,1)-YDIFF).LE.0.1D-3.AND.
      3DABS(MUTARA(K,2)-XDIFF).LE.0.1D-3)) GO TO 20
    10 CONTINUE
       WRITE(6,100) XDIFF,YDIFF
   100 FORMAT(1X,'NO MATCH FOR ',F5.2,' , ',F5.2,' CASE.',/)
       RMUT = XMUT = 0.0
       RETURN
    20 RMUT = MUTARA(K,3)
       XMUT = MUTARA(K,4)
       RETURN
       END
C SUBROUTINE TO FIND THE RADIATION IMPEDANCE PARAMETERS
C   THETA NOUGHT AND XI NOUGHT AS USED IN EQUATION 7.4.44
C   OF MORSE AND INGARD'S BOOK, 'THEORETICAL ACOUSTICS'
       SUBROUTINE RADIMP(FREQ,LENGTH,THNOT,XINOT)
       REAL*8 GAMMA,THNOT,XINOT,MMBSJ1,PI,ANS,FREQ,LENGTH
       DATA SSPEED/.15D+04/
       PI = 4.0*DATAN(1.0D00)
       GAMMA = 2. * PI * FREQ * LENGTH / SSPEED
       CALL INTGR1(0.0D00,PI/2.,3,20,GAMMA,ANS)
       XINOT = 4.0 * ANS/PI
       THNOT = 1-(2./GAMMA)*MMBSJ1(GAMMA,IER)
       RETURN
       END
C     SUBROUTINE TO FIND THE MUTUAL INTERACTION COEFFICIENTS
C     FOR ANY COMBINATION OF POSITIONS.
C     THE OUTPUT IS PUT IN THE ARRAY MUTARA,
C     WHICH CONTAINS THE X-OFFSET, Y-OFFSET, REAL, AND
C     IMAGINARY INTERACTION COEFFICIENTS.
       SUBROUTINE FINDMT(FREQ,LENGTH)
       REAL*8 CA,CB,CG,CH,C,A,B,G,H,MUTARA(35,4),SSPEED
       REAL*8 FREQ,LENGTH
       COMMON/MUTUAL/MUTARA
       DATA SSPEED/.15D+04/
       C = 8. * DATAN(1.0 D0)*FREQ/SSPEED
       A = B = 1.0
       H = G = 0.0
       L = 0
       DO 6 I=2,8
       DO 5 K = 1,I
       L = L + 1
       G = MUTARA(L,1) = DFLOAT(I-1)
       H = MUTARA(L,2) = DFLOAT(K-1)
       CA = C * A*LENGTH
       CB = C * B*LENGTH
```

```
      CG = C * G*LENGTH
      CH = C * H*LENGTH
      CALL MUTIMP(CA,CB,CG,CH,MUTARA(L,3),MUTARA(L,4))
    5 CONTINUE
    6 CONTINUE
      RETURN
      END
C SUBROUTINE TO FIND THE REAL AND REACTIVE PARTS OF THE
C MUTUAL IMPEDANCE RM AND XM, GIVEN THE ALPHA,BETA,G, AND H
C AS DESCRIBED IN ARASE.
      SUBROUTINE MUTIMP(CKA,CKB,CKG,CKH,R,X)
      REAL*8 CKA,CKB,CKH,CKG,R,X,CONST1(9),CONST2(9),
     1CONST3(9),TOTC,TOTS,PI,C,S
      DATA CONST1/4.0,4*-2.0,4*1.0/
      DATA CONST2/0.0,-1.0,0.0,1.0,0.0,2*-1.0,2*1.0/
      DATA CONST3/2*0.0,-1.0,0.0,1.0,-1.0,1.0,-1.0,1.0/
      PI = 4.*DATAN(1.0 DO)
      TOTS =TOTC = 0.0 DO
      DO 1 K=1,9
      CALL CANDS(CKH+CONST2(K)*CKA,CKG+CONST3(K)*CKB,C,S)
      TOTC = TOTC + C*CONST1(K)
    1 TOTS = TOTS + S*CONST1(K)
      R = TOTC/(2.*PI*CKA*CKB)
      X = TOTS/(2.*PI*CKA*CKB)
      RETURN
      END
C SUBROUTINE TO FIND BOTH C(X,Y) AND S(X,Y) AT THE SAME TIME
      SUBROUTINE CANDS(A,B,C,S)
      REAL*8 A,B,C,S,QUANTP,ABSA,ABSB,DCOS,DSIN,OUT(2),
     1PLMULT(2),OUT1,OUT2
      DATA PLMULT/1.0 ,-1.0/
      QUANTP = DSQRT(A * A + B * B)
      ABSA = DABS(A)
      ABSB = DABS(B)
      N=15
      DO 1  K=1,2
      CALL INTGR1(ABSB,QUANTP,N,K,B,OUT1)
      CALL INTGR1(ABSA,QUANTP,N,K,A,OUT2)
      OUT(K) = PLMULT(K)*(ABSA*OUT1 + ABSB*OUT2)
    1 CONTINUE
      C = OUT(1) - DCOS(QUANTP) - QUANTP*DSIN(QUANTP)
      S = OUT(2) - QUANTP*DCOS(QUANTP) + DSIN(QUANTP)
      RETURN
      END
C INTEGRAND FROM MORSE AND INGARD'S EQ 7.4.44 AND ARASE PAPER
      DOUBLE PRECISION FUNCTION CKERNL(Q,N,PARAM)
      REAL*8 Q,PARAM,QUANTM,CHECK
      CHECK = Q * Q - PARAM * PARAM
      IF (CHECK.GE.0.0 DO) GO TO 10
      CHECK = 0.0 DO
   10 QUANTM = DSQRT(CHECK)
      IF (FLOAT(N) - 2.) 1,2,3
C     INTEGRAND FOR C(X,Y)
    1 CKERNL = DCOS(Q) * QUANTM / Q
```

```
      RETURN
C     INTEGRAND FOR S(X,Y)
    2 CKERNL = DSIN(Q) * QUANTM / Q
      RETURN
C     INTEGRAND FOR STRUVE FUNCTION
    3 CKERNL = DSIN(PARAM*DCOS(Q))*(DSIN(Q))**2.
      RETURN
      END
C INTEGRATION SUBROUTINE
      SUBROUTINE INTGR1(XL,XU,N,NPARM,PASS,ANS)
      REAL*8 ANS,H,XL,XU,CKERNL,GAUSS,DFLOAT,PASS
      EXTERNAL CKERNL,GAUSS
      ANS = 0.
      H = (XU-XL)/DFLOAT(N)
      IF(H.LE.0.0 D0) GO TO 2
      DO 1 I=1,N
    1 ANS=ANS+GAUSS(XL+(DFLOAT(I)-1.)*H,XU-
     1(DFLOAT(N)-DFLOAT(I))*H,NPARM,PASS)
      RETURN
    2 ANS = 0.0 D0
      RETURN
      END
C GAUSSIAN ROUTINE
      DOUBLE PRECISION FUNCTION GAUSS(X1,X2,MPARM,PASS)
      REAL*8 X1,X2,T,E,C,CKERNL,PASS,CONST
      EXTERNAL CKERNL
      DATA CONST/0.1127016653792583D+00/
      T = X2 + X1
      E = X2 - X1
      C = CONST * E
      GAUSS= E/18.*(5.*CKERNL(C+X1,MPARM,PASS)+8.*CKERNL(T/2.,
     1MPARM,PASS)+5.*CKERNL(X2-C,MPARM,PASS))
      RETURN
      END
```

BIBLIOGRAPHY

1. Kendig, P. M., Notes on Selecting Element Positions in an Array, personal communication.

2. McCammon, D. F. and Thompson, W., "The Design of Tonpilz Piezoelectric Transducers Using Nonlinear Goal Programming," J. Acoust. Soc. Am., 68, 754-757 (1980)

3. Martin, G. E. "On the Theory of Segmented Electromechanical Systems," J. Acoust. Soc. Am., 36, 1366-1370 (1964)

4. Kinsler, L. E. and Frey, A. R., Fundmentals of Acoustics, Second Edition, John Wiley and Sons, New York, Ch. 12, 1968.

5. Cherpak, V. A., "Dynamic Lumped Parameters of Composite Piezoelectric Transducers," Sov. Phys. Acoust., 23, #3,246-250 (1977)

6. Butler, J. L., Cipolla, T. R., and Brown, W. D., "Radiating Head Flexure and It's Effect on Transducer Performance", J. Acoust. Soc. Am., 70, 500-503 (1981)

7. Hayt, W. H., Jr. and Kemmerly, J. E., Engineering Circuit Analysis McGraw-Hill, New York, 1971. Chapter 16

8. Lagrace, L. J. and Kissinger, C. D. "Non-Contacting Displacement and Vibration Measurement Systems Employing Fiber Optic and Capacitive Techniques". Presented at the 23rd International Intrumentation Symposium, May 1977, Las Vegas (ISA Reprint)

9. Albers,Vernon M. Underwater Acoustics Handbook II Pensylvania State University Press, University Park, 1965. Chapter 21

10. American National Standards Institute, Procedure for Calibration of Underwater Electroacoustic Transducers, ANSI S1.20-1972

11. Draus, S. M., "The Design of Acoustic Transducer Arrays Using Goal Programming." Master of Science Thesis in Industrial Engineering, Pensylvania State University, August 1977.

12. Ignizio, J. P., Goal Programming and Extensions. D. C. Heath & Co. Lexington, Ma. (1976)

13. Morse, P. M. and Ingard, K. U., Theoretical Acoustics McGraw-Hill, New York, 1968.

14. Funderlic, R. E., The Programmer's Handbook, American Data Processing, Detroit, 1969. p 53

15. Arase, E. M., "Mutual Radiation Impedance of Square and Rectangular Pistons in a Rigid Infinite Baffle." J. Acoust. Soc. Am., 36, 1521-1525 (1964)

16. Kendig, P. M. Notes on Element Tolerance Studies, pesonal communication.

DISTRIBUTION LIST FOR TM 82-62

Commander (NSEA 0342)
Naval Sea Systems Command
Department of the Navy
Washington, DC 20362

Copies 1 and 2

Commander (NSEA 9961)
Naval Sea Systems Command
Department of the Navy
Washington, DC 20362

Copies 3 and 4

Defense Technical Information Center
5010 Duke Street
Cameron Station
Alexandria, VA 22314

Copies 5 through 10

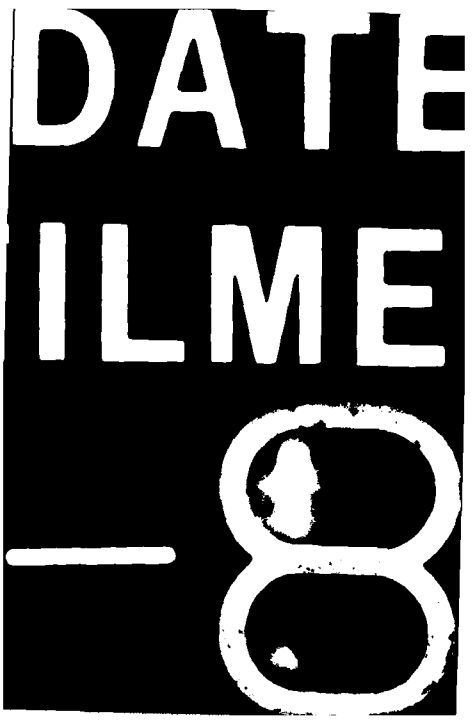
DATE
ILME
8